J. Phys. B: At. Mol. Opt. Phys. **22** (1989) 3551-3586. Printed in the UK

TOPICAL REVIEW

# Spectroscopy of the hydrogen molecular ion

Alan Carrington, Iain R McNab and Christine A Montgomerie

Department of Chemistry, University of Southampton, Hampshire SO9 5NH, UK

**Abstract.** The theory and spectroscopy of the hydrogen molecular ion in its isotopic forms $H_2^+$, $HD^+$ and $D_2^+$ is reviewed. Theoretical treatments are directed towards the calculation of potential energy curves, vibration-rotation energies and nuclear hyperfine constants. In the Born-Oppenheimer approximation the Schrödinger equation for $H_2^+$ can be solved exactly, but further approximations (adiabatic or non-adiabatic) must be developed to describe the coupling of electronic and nuclear motion. The lack of a centre of symmetry in $HD^+$ creates particular difficulties in the theory.

Radiofrequency hyperfine transitions have been measured for $H_2^+$ using quadrupole trapping and photoalignment. Ion beam methods have been used to measure vibration-rotation transitions in $HD^+$, and particular attention has been paid to levels very close to the dissociation limit. Analysis of proton and deuteron nuclear hyperfine structure reveals extreme asymmetry of the electron distribution in these levels. The hyperfine interactions have been measured with high precision by radiofrequency/infrared and microwave/infrared double resonance experiments. The results show that $HD^+$ in ground-state vibration-rotation levels close to the dissociation limit may be regarded as a $D\cdots H^+$ long-range complex.

The first excited electronic state of $H_2^+$ is repulsive at internuclear distances less than 5 Å but exhibits a shallow minimum at larger internuclear distances because of the attractive charge/induced-dipole interaction between the proton and the hydrogen atom. This minimum is calculated to support a small number of stable vibration-rotation levels. An electronic spectrum of $D_2^+$ arising through excitation from the ground electronic state to the excited long-range state has been measured using both infrared and microwave radiation, and the $D\cdots D^+$ long-range complex has been fully characterised. Observation of a microwave electronic transition in $H_2^+$ has provided experimental identification of the related $H\cdots H^+$ long-range complex.

## 1. Introduction

The hydrogen molecular ion $H_2^+$ and its isotopic relations $HD^+$ and $D_2^+$ have played important roles in the development of molecular quantum mechanics. $H_2^+$ has been regarded as a model system for the formulation of many different methods and approximations, and the absence of interelectron interactions has enabled other aspects of molecular structure theory to be examined in depth. We probably understand the structure and dynamics of the hydrogen molecular ion better than those of any other molecule. $H_2^+$ is, however, much easier to study theoretically than experimentally, and although its physical properties have been extensively calculated, few have been measured. It is an elusive molecule in the laboratory because, although it has a large binding energy and is therefore thermodynamically stable, it is very reactive, particularly towards molecular hydrogen. Since $H_2^+$ is usually formed by direct ionisation of $H_2$, it is necessary to design experiments in which the ion is separated rapidly from its neutral parent.

Many of the physical properties of the hydrogen molecular ion could, in principle, be measured by spectroscopic methods, but even if the chemical problem of its isolation can be solved satisfactorily, other difficulties remain. The homonuclear species $H_2^+$

0953-4075/89/223551+36$02.50  

and $D_2^+$ do not possess electric dipole moments, so that they cannot exhibit electric-dipole-allowed vibrational or rotational spectra. Only the mixed isotope species, $HD^+$, satisfies this requirement and consequently has been studied much more thoroughly than its homonuclear relatives. Studies of the electronic spectra would be possible if suitable excited electronic states existed. However, the lowest excited electronic state of $H_2^+$ is essentially repulsive, and the higher excited states lie more than 11 eV above the ground state. Electronic transitions between the ground and highly excited states would therefore occur in the far vacuum ultraviolet. They would also have very poor Franck-Condon factors, because the potential minimum for the ground state occurs at a very small value of the internuclear distance, compared with those calculated for the excited states.

We have made considerable progress with these spectroscopic problems during the past ten years, as we shall describe. Only two other direct spectroscopic studies of the hydrogen molecular ion have been described. The first was a beautiful radiofrequency study of $H_2^+$ using quadrupole trapping and photoalignment (Richardson *et al* 1968). The second was the measurement of the vibration-rotation spectrum of $HD^+$ in its lowest vibrational levels by an ingenious ion beam method (Wing *et al* 1976). The details of these experiments are described in § 4. Most of the previous experimental knowledge of $H_2^+$ and its isotopes has come from indirect studies, such as the photoelectron, photoionisation and Rydberg spectroscopy of $H_2$. Some of these studies were landmarks in the development of molecular spectroscopy, but this review is concerned only with *direct* spectroscopic methods. The relevant theory is described briefly in §§ 2 and 3, but for deeper discussions of the theory the reader must look elsewhere. The predictions and results of the theoretical studies are examined in detail, however, because much of our motivation has been to develop experiments which subject the theory to stringent tests.

## 2. Theory of electronic states, potential curves and energy levels

The Schrödinger equation for the hydrogen molecular ion may be solved at many different levels of approximation. In what follows we distinguish between three types of solution; the Born-Oppenheimer solution (which we define as the solution for motion of the electron in the field of the clamped nuclei), adiabatic solutions which include only terms in the coupling between nuclear and electronic motion which are diagonal in the electronic states and non-adiabatic solutions. Both the Born-Oppenheimer and adiabatic approaches separate nuclear and electronic motion, leading to the concept of electronic potential energy curves and separated electronic states.

### *2.1. The full non-relativistic Hamiltonian*

The complete non-relativistic Hamiltonian for a system of point charges interacting electrostatically may be written as

$$\mathscr{H} = \sum_i \frac{-\hbar^2 \nabla_i^2}{2m_i} - \sum_i \sum_{j>i} \frac{z_i z_j e^2}{4\pi\varepsilon_0 r_{ij}} \tag{1}$$

where all symbols have their usual meanings, and the coordinates are in the laboratory frame. Separation of the translational motion of the particles may be achieved by

several transformations, but we choose to transform from the laboratory frame to the geometric centre of the nuclei. In matrix form the transformation and its inverse are

$$\begin{bmatrix} \boldsymbol{r}_g \\ \boldsymbol{R} \\ \boldsymbol{R}_{cm} \end{bmatrix} = \begin{bmatrix} -\frac{1}{2} & -\frac{1}{2} & 1 \\ -1 & 1 & 0 \\ m_1/M & m_2/M & m_e/M \end{bmatrix} \begin{bmatrix} \boldsymbol{r}_1 \\ \boldsymbol{r}_2 \\ \boldsymbol{r}_e \end{bmatrix}$$
$$\begin{bmatrix} \boldsymbol{r}_1 \\ \boldsymbol{r}_2 \\ \boldsymbol{r}_e \end{bmatrix} = \begin{bmatrix} -m_e/M & -(m_2+\frac{1}{2}m_e)/M & 1 \\ -m_e/M & (m_1+\frac{1}{2}m_e)/M & 1 \\ M_n/M & \frac{1}{2}(m_1-m_2)/M & 1 \end{bmatrix} \begin{bmatrix} \boldsymbol{r}_g \\ \boldsymbol{R} \\ \boldsymbol{R}_{cm} \end{bmatrix} \tag{2}$$

where $M = m_1 + m_2 + m_e$ and $M_n = m_1 + m_2$. The coordinate vectors are illustrated in figure 1. The new basis vectors are the internuclear vector $\boldsymbol{R}$, the position of the centre of mass relative to the space-fixed origin $\boldsymbol{R}_{cm}$ and the position of the electron relative to the geometric centre of the nuclei $\boldsymbol{r}_g$.

The electrostatic potential energy between the particles is given by

$$V = \frac{e^2}{4\pi\varepsilon_0}\left[\frac{1}{R} - \frac{1}{r_{1e}} - \frac{1}{r_{2e}}\right]. \tag{3}$$

$V$ is unchanged by the transformation (2), since it depends only upon the relative positions of the particles. However, the kinetic energy operator in the Hamiltonian (1) is transformed to

$$T = -\hbar^2\left[\frac{\nabla_g^2}{2m_e} + \frac{\nabla_R^2}{2\mu} + \frac{\nabla_g^2}{8\mu} + \frac{\boldsymbol{\nabla}_g \cdot \boldsymbol{\nabla}_R}{2\mu_a} + \frac{\nabla_{cm}^2}{2M}\right] \tag{4}$$

where $1/\mu = (1/m_1) + (1/m_2)$ and $1/\mu_a = (1/m_1) - (1/m_2)$. The motion of the centre of mass is contained in the $\nabla_{cm}^2$ term, and may be separated out, leaving the Schrödinger equation for the internal motions of the molecule,

$$\left\{-\hbar^2\left[\frac{\nabla_g^2}{2m_e} + \frac{\nabla_R^2}{2\mu} + \frac{\nabla_g^2}{8\mu} + \frac{\boldsymbol{\nabla}_g \cdot \boldsymbol{\nabla}_R}{2\mu_a}\right] + V\right\}\psi_{mol} = E_{int}\psi_{mol}. \tag{5}$$

The various levels of approximation at which this equation may be solved are now discussed.

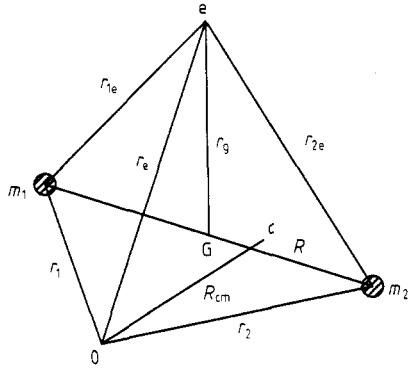


**Figure 1.** Electron and nuclear coordinates used in the transformation of the origin from the laboratory frame to the geometric centre of the nuclei.

*2.2. The electronic Born–Oppenheimer solution*

The $\nabla_g \cdot \nabla_R/2\mu_a$ term in equation (5) couples the electronic and nuclear motions, making exact solution impossible. Approximations must therefore be made to make the problem tractable. The first such approximation is to solve the Schrödinger equation for the motion of the electron in the electrostatic field of the clamped nuclei. This yields the electronic Born–Oppenheimer equation,

$$(-\hbar^2\nabla_g^2/2m_e + V)\varphi_t = E_t\varphi_t \tag{6}$$

where $\varphi_t$ and $E_t$ are labelled according to the electronic state $t$. In a prolate spheroidal coordinate system, equation (6) is separable and gives rise to three one-dimensional differential equations, which may be solved exactly with series expansions (Jaffé 1934, Hylleraas 1931). The prolate spheroidal coordinates are defined by

$$\begin{aligned} \xi &= (r_{1e} + r_{2e})/R \qquad \text{with} \quad 1 \leqslant \xi < \infty \\ \eta &= (r_{1e} - r_{2e})/R \qquad \text{with} \quad -1 \leqslant \eta \leqslant 1 \end{aligned} \tag{7}$$

and $\chi$ is the rotation of the electron about the internuclear ($z$) axis ($0 \leqslant \chi < 2\pi$). This allows the electronic Born–Oppenheimer equation to be written (in atomic units),

$$\left[\frac{\partial}{\partial\xi}(\xi^2-1)\frac{\partial}{\partial\xi} + \frac{\partial}{\partial\eta}(1-\eta^2)\frac{\partial}{\partial\eta} + \left(\frac{1}{(\xi^2-1)} + \frac{1}{(1-\eta^2)}\right)\frac{\partial^2}{\partial\chi^2} + 2R\xi - p^2(\xi^2-\eta^2)\right]\varphi_t = 0 \tag{8}$$

where $\varphi_t = \varphi(R, \xi, \eta, \chi)$ and $p^2 = -\frac{1}{2}[E_t(R) - (1/R)]R^2$. Using the substitution

$$\varphi_t(R, \xi, \eta, \chi) = L(R, \xi)M(R, \eta)N(\chi) \tag{9}$$

we obtain the separated equations

$$\left(\frac{\partial^2}{\partial\chi^2} + \Lambda^2\right)N = 0 \tag{10}$$

$$\left(\frac{\partial}{\partial\xi}(\xi^2-1)\frac{\partial}{\partial\xi} + A - \frac{\Lambda^2}{(\xi^2-1)} + 2R\xi - p^2\xi^2\right)L = 0 \tag{11}$$

$$\left(\frac{\partial}{\partial\eta}(1-\eta^2)\frac{\partial}{\partial\eta} - A - \frac{\Lambda^2}{(1-\eta^2)} + p^2\eta^2\right)M = 0 \tag{12}$$

where $\Lambda^2$ and $A$ are the separation constants.

The $\chi$ equation can be solved analytically, giving

$$N(\chi) = \exp(i\Lambda\chi)/(2\pi)^{1/2} \tag{13}$$

with $\Lambda = 0, \pm1, \pm2 \ldots$ For the solution of the $\xi$ equation we use the Jaffé expansion

$$L(R, \xi) = (\xi^2-1)^{\Lambda/2}(\xi+1)^{\sigma}\exp(-p\xi)\sum_{n=0}^{\infty} g_n(R)[(\xi-1)/(\xi+1)]^n \tag{14}$$

where $\sigma = (R/p) - \Lambda - 1$. The $\eta$ equation may be solved using an expansion over associated Legendre functions

$$M(R, \eta) = \sum_{s=0}^{\infty} f_s(R)P_{\Lambda+s}^{\Lambda}(\eta). \tag{15}$$

Substituting these expansions in (11) and (12) yields recursion relations, which may be expressed as matrix eigenvalue equations (Hunter and Pritchard 1967, p 2146). The

overall solution is achieved for a given $R$ value by requiring that $A$ simultaneously satisfies both equations. Solution of the Born-Oppenheimer equation yields an electronic potential energy curve, $U(R) = E_t(R)$, in which all couplings between nuclear and electronic motion have been neglected. The radial Schrödinger equation for the nuclear motion is then

$$\left(-\frac{d^2}{dR^2}+\frac{2\mu}{\hbar^2}(U(R)-E_{vN})+\frac{N(N+1)}{R^2}\right)\chi_{vN}(R)=0 \tag{16}$$

and its vibration-rotation eigenfunctions and eigenenergies may be found by Numerov-Cooley integration (Cooley 1961). An excellent introduction to the numerical solution of the Born-Oppenheimer equation is given by Teller and Sahlin (1970).

### *2.3. The standard adiabatic approximation*

Considering once more the full internal Hamiltonian in (5), we see that possible solutions might be expressed as series expansions over the Born-Oppenheimer solutions ($\varphi_t$) (Born and Huang 1954),

$$\psi_{\text{mol}}(\boldsymbol{R}, \boldsymbol{r}_g)=\sum_t F_t(\boldsymbol{R})\varphi_t(R, \boldsymbol{r}_g). \tag{17}$$

Substituting (17) into the Schrödinger equation for internal motions (5) yields a set of coupled differential equations for the functions $F_t(\boldsymbol{R})$

$$\mathscr{H}_{\text{int}}\sum_t F_t(\boldsymbol{R})\varphi_t(R, \boldsymbol{r}_g)=E_{\text{int}}\sum_t F_t(\boldsymbol{R})\varphi_t(R, \boldsymbol{r}_g). \tag{18}$$

Premultiplying by $\varphi_s^*(R, \boldsymbol{r}_g)$ and integrating over the electronic coordinate $\boldsymbol{r}_g$ gives

$$E_s(R)F_s(\boldsymbol{R})+\sum_t\int\varphi_s^*(R, \boldsymbol{r}_g)\left(-\frac{\nabla_R^2}{2\mu}-\frac{\nabla_g^2}{8\mu}-\frac{\boldsymbol{\nabla}_g\cdot\boldsymbol{\nabla}_R}{2\mu_a}\right)F_t(\boldsymbol{R})\varphi_t(R, \boldsymbol{r}_g)\,d\boldsymbol{r}_g=E_{\text{int}}F_s(\boldsymbol{R}). \tag{19}$$

In the Born-Oppenheimer equation, the nuclei are treated as point charges, and hence the functions $\varphi_t(R, \boldsymbol{r}_g)$ are either symmetric or antisymmetric under exchange of nuclei and electron inversion through the geometric centre of the nuclei. Using these symmetry operations enables (19) to be written in the form

$$\begin{aligned}\left[E_s(R)-\frac{\nabla_R^2}{2\mu}-\int\varphi_s^*(R, \boldsymbol{r}_g)\left(\frac{\nabla_g^2}{8\mu}+\frac{\nabla_R^2}{2\mu}\right)\varphi_s(R, \boldsymbol{r}_g)\,d\boldsymbol{r}_g\right]F_s(\boldsymbol{R})\\ +\sum_{t\neq s}\left[\int\varphi_s^*(R, \boldsymbol{r}_g)\left(-\frac{\nabla_g^2}{8\mu}-\frac{\nabla_R^2}{2\mu}-\frac{\boldsymbol{\nabla}_g\cdot\boldsymbol{\nabla}_R}{2\mu_a}\right)\varphi_t(R, \boldsymbol{r}_g)\,d\boldsymbol{r}_g\right.\\ \left.+\int\varphi_s^*(R, \boldsymbol{r}_g)\left(-\frac{\boldsymbol{\nabla}_R}{\mu}-\frac{\boldsymbol{\nabla}_g}{2\mu_a}\right)\varphi_t(R, \boldsymbol{r}_g)\,d\boldsymbol{r}_g\cdot\boldsymbol{\nabla}_R\right]F_t(\boldsymbol{R})=E_{\text{int}}F_s(\boldsymbol{R}).\end{aligned} \tag{20}$$

This infinite set of coupled differential equations cannot be solved exactly; the standard adiabatic approximation consists of neglecting all but the diagonal couplings, leaving only

$$\begin{aligned}\left(E_s(R)-\int\varphi_s^*(R, \boldsymbol{r}_g)\frac{\nabla_g^2}{8\mu}\varphi_s(R, \boldsymbol{r}_g)\,d\boldsymbol{r}_g-\int\varphi_s^*(R, \boldsymbol{r}_g)\frac{\nabla_R^2}{2\mu}\varphi_s(R, \boldsymbol{r}_g)\,d\boldsymbol{r}_g-\frac{\nabla_R^2}{2\mu}\right)F_s^{\text{AD}}(\boldsymbol{R})\\ =E_{\text{int}}^{\text{AD}}F_s^{\text{AD}}(\boldsymbol{R}).\end{aligned} \tag{21}$$

This is equivalent to defining an effective potential

$$U(R) = E_s(R) - \int \varphi_s^*(R, \boldsymbol{r}_g) \frac{\nabla_g^2}{8\mu} \varphi_s(R, \boldsymbol{r}_g)\, d\boldsymbol{r}_g - \int \varphi_s^*(R, \boldsymbol{r}_g) \frac{\nabla_R^2}{2\mu} \varphi_s(R, \boldsymbol{r}_g)\, d\boldsymbol{r}_g \qquad (22)$$

which may again be substituted into (16) to obtain $\chi_{vN}$, $E_{vN}$. The standard adiabatic correction therefore consists of retaining the diagonal corrections, improving the approximation while still effectively separating the electronic and nuclear motions. Calculations for $H_2^+$, $HD^+$ and $D_2^+$ have been tabulated by Hunter *et al* (1974). For $HD^+$, the $\nabla_g \cdot \nabla_R / 2\mu_a$ term couples the ground ($1s\sigma$) and first excited ($2p\sigma$) electronic states ($1/\mu_a = 0$ for the homonuclear molecules); thus the symmetry is broken and there are two possible dissociation limits, $H^+ + D$ and $H + D^+$, which differ in energy by $29.8\ cm^{-1}$. The standard adiabatic approximation fails to discriminate between these limits, leading to serious errors in vibration-rotation energies calculated near dissociation. The consequences of this non-degeneracy are explored further in § 4.

### *2.4. Improved adiabatic calculations*

An improved adiabatic approach to the problem of $HD^+$ has been developed by Pack and co-workers (Pack 1985, Struensee *et al* 1986). The Hamiltonian used correctly accounts for the non-degenerate dissociation limits of $HD^+$, but prevents the separation of variables, and hence a variational solution is required. Vibrational energies were calculated only for $N = 0$, but the method correctly predicted that $v = 22$ is the highest bound level of $HD^+$.

### *2.5. Matrix elements of the Hamiltonian*

In order to apply the formal Hamiltonian in (20) to the hydrogen molecular ion and therefore to determine the adiabatic and non-adiabatic corrections, we require it to be expressed in terms of the internal coordinates of the system. This can be achieved by means of several transformations similar in nature to those given in (2); both the matrix elements and their explicit derivations are given by Carrington and Kennedy (1984).

### *2.6. Non-adiabatic approximations*

The non-adiabatic problem is insoluble when expressed in the form of (20). We regard any attempt at a solution of the problem which accounts for off-diagonal coupling of the electronic states to be non-adiabatic.

One solution is to reduce the problem by considering only a finite number of coupled states, terminating the Born expansion in the hope of rapid convergence. Hunter and Pritchard (1967, p 2153) calculated the four lowest vibrational states of $H_2^+$, $D_2^+$ and $HD^+$ in this fashion, finding initial rapid convergence. Much longer expansions would be required for higher vibrational levels, and alternative formulations of the problem are more fruitful.

*2.6.1. Variational approaches.* Accurate variational calculations have been performed by Bishop (1974), and Bishop and Cheung (1977). The eigenenergies of the complete Hamiltonian were found by variational adjustment of a trial wavefunction. Only a few low-lying levels of the ground electronic state were considered. The final results, obtained with up to 515 term expansions, were considered to be accurate to within

$\pm 0.001\ \mathrm{cm}^{-1}$ after inclusion of radiative and relativistic corrections. Kohl and Shipsey (1986) calculated vibrational levels to dissociation for $H_2^+$, but with low accuracy. It is possible that the accuracy of their method can be improved.

*2.6.2. Coupled-states approach.* This approach lifts the degeneracy of the standard adiabatic dissociation limits in $HD^+$, by considering the required behaviour of the electronic wavefunctions close to dissociation. Carrington and Kennedy (1985) formed suitably asymmetric electronic wavefunctions for the $1s\sigma$ and $2p\sigma$ states of $HD^+$ by considering normalised linear combinations of the $1s\sigma_g(\varphi_1)$ and $2p\sigma_u(\varphi_2)$ adiabatic states,

$$\Phi_{1s\sigma} = a\varphi_1 + b\varphi_2 \qquad \Phi_{2p\sigma} = b\varphi_1 - a\varphi_2. \tag{23}$$

The $1s\sigma_g$ and $2p\sigma_u$ states are mixed by the operator which couples nuclear and electronic motion in the Hamiltonian $(-\nabla_g \cdot \nabla_R/2\mu_a)$. Ignoring other electronic states (which are far removed in energy) and evaluating the matrix element of this term between the two adiabatic states, using matrix elements of the complete Hamiltonian, gives a submatrix which may be decomposed to

$$\mathscr{H}(R) = \begin{pmatrix} U^{\mathrm{AD}}_{1s\sigma}(R) & H(R) \\ H(R) & U^{\mathrm{AD}}_{2p\sigma}(R) \end{pmatrix} + \begin{pmatrix} 0 & A(R) \\ -A(R) & 0 \end{pmatrix} \tag{24}$$

where

$$\begin{aligned} H(R) &= \tfrac{1}{2}\int \Phi^*_{1s\sigma}\mathscr{H}_{\mathrm{int}}\Phi_{2p\sigma}\,\mathrm{d}\boldsymbol{r}_g + \tfrac{1}{2}\int \Phi^*_{2p\sigma}\mathscr{H}_{\mathrm{int}}\Phi_{1s\sigma}\,\mathrm{d}\boldsymbol{r}_g \\ A(R) &= \tfrac{1}{2}\int \Phi^*_{1s\sigma}\mathscr{H}_{\mathrm{int}}\Phi_{2p\sigma}\,\mathrm{d}\boldsymbol{r}_g - \tfrac{1}{2}\int \Phi^*_{2p\sigma}\mathscr{H}_{\mathrm{int}}\Phi_{1s\sigma}\,\mathrm{d}\boldsymbol{r}_g. \end{aligned} \tag{25}$$

Diagonalising only the Hermitian matrix yields the mixing coefficients $a$ and $b$ at a given $R$ value. Averaging the full Hamiltonian over the mixed wavefunctions gives effective potential curves which correlate correctly with the dissociation limits.

*2.6.3. Transformed Hamiltonian treatment for $HD^+$.* Moss and Sadler (1987, 1988, 1989) have developed another means of dealing with the non-degenerate dissociation limits of $HD^+$. Their method is superior to the coupled-states approach in that it accounts correctly for *all* the dissociation limits of $HD^+$, and implicitly accounts for couplings between *all* g and u states. This is achieved by successive unitary transformations of the Hamiltonian for $HD^+$, of the form $e^{iS}\mathscr{H}e^{-iS}$, where the exponential operators are to be considered as series. This is similar in conception to the Foldy-Wouthuysen transformations used to transform the Dirac Hamiltonian (see, for example, Moss 1973), resulting in a series of nested commutators. The operators $S$ are chosen such that terms coupling nuclear and electronic motion are removed, resulting in additional potential terms because of the transformation of the potential energy, $i[S, V]$. This effectively repartitions the asymmetry of the Hamiltonian into the electrostatic potential energy, and may be interpreted as introducing a slight asymmetry into the nuclear charges of the two nuclei ($Z_1 = 0.999\,9319$, $Z_2 = 1.000\,0680$). The electronic equation is solved variationally, using basis functions modelled on the Hylleraas expansion. Results were found to be in close agreement with calculations in the coupled-states approximation (Kennedy *et al* 1988).

The transformed Hamiltonian method gives the correct united atom limit, the correct dissociation limits for all states, and the correct separated-atom electron densities. The most attractive features of this approximation are that it allows for coupling of all g and u states and introduces a simple physical interpretation of the resulting Hamiltonian.

*2.6.4. Variation-perturbation approximation.* This method was developed by Wolniewicz and Poll (1978, 1980, 1985, 1986). They treated non-adiabatic effects as a perturbation on the adiabatic approximation. This allows the adiabatic wavefunctions, which are easily obtained, to be used as a starting point for the calculation.

A formal adiabatic Hamiltonian is defined

$$\mathscr{H}^{\mathrm{ad}} = \sum_n E_n^{\mathrm{ad}} |\psi_n^{\mathrm{ad}}\rangle\langle\psi_n^{\mathrm{ad}}| \tag{26}$$

where $E_n^{\mathrm{ad}}$ are the adiabatic energies and $|\psi_n^{\mathrm{ad}}\rangle$ are a complete set of adiabatic eigenfunctions, given by

$$\psi_n^{\mathrm{ad}} = \varphi_n^{\mathrm{BO}}(R, \boldsymbol{r}_{\mathrm{g}}) F_n^{\mathrm{ad}}(R). \tag{27}$$

$F_n^{\mathrm{ad}}(R)$ is a solution of the radial Schrödinger equation with $U(R)$ equal to the adiabatic potential. $\varphi_n^{\mathrm{BO}}(R, \boldsymbol{r}_{\mathrm{g}})$ are solutions of the electronic Born-Oppenheimer equation. The total Hamiltonian can now be separated into $\mathscr{H}^{\mathrm{ad}}$ as defined above and a term, $\mathscr{H}^{\mathrm{nad}}$, which is to be treated as a perturbation:

$$\mathscr{H} = \mathscr{H}^{\mathrm{ad}} + \mathscr{H}^{\mathrm{nad}}. \tag{28}$$

This means that

$$\mathscr{H}|\psi_n^{\mathrm{ad}}\rangle = E_n^{\mathrm{ad}}|\psi_n^{\mathrm{ad}}\rangle + \mathscr{H}^{\mathrm{nad}}|\psi_n^{\mathrm{ad}}\rangle \tag{29}$$

and as $\langle\psi_n^{\mathrm{ad}}|\mathscr{H}|\psi_n^{\mathrm{ad}}\rangle = E_n^{\mathrm{ad}}$, the first-order energy correction is zero:

$$\langle\psi_n^{\mathrm{ad}}|\mathscr{H}^{\mathrm{nad}}|\psi_n^{\mathrm{ad}}\rangle = 0. \tag{30}$$

To find the second-order energy correction, $\psi^{\mathrm{ad}}$ is treated as the zero-order eigenfunction and the first-order eigenfunction is written

$$\psi_n = \psi_n^{\mathrm{ad}} + \psi_n' \tag{31}$$

where $\psi_n$ satisfies the equation

$$(\mathscr{H}^{\mathrm{ad}} - E_n^{\mathrm{ad}})\psi_n' = -\mathscr{H}^{\mathrm{nad}}\psi_n^{\mathrm{ad}}. \tag{32}$$

The second-order energy correction is given by

$$E'' = \langle\psi_n'|\mathscr{H}^{\mathrm{nad}}|\psi_n^{\mathrm{ad}}\rangle = \langle\psi_n'|\mathscr{H} - E_n^{\mathrm{ad}}|\psi_n^{\mathrm{ad}}\rangle. \tag{33}$$

This second equality reintroduces the differential operators. To first order the ground state only couples to the excited $\Sigma$ and $\Pi$ states. The non-adiabatic corrections are computed independently for each coupling,

$$E'' = \sum_{\Lambda\alpha} E''_{\Lambda\alpha} \tag{34}$$

where $\Lambda$ is the projection of the orbital angular momentum on the internuclear axis and $\alpha$ includes the g and u corrections. For the $HD^+$ $1s\sigma$ ground state this is

$$\Delta E^{\mathrm{nad}} = E''_{0,\mathrm{g}} + E''_{0,\mathrm{u}} + 2E''_{1,\mathrm{g}} + 2E''_{1,\mathrm{u}}, \tag{35}$$

since $E''_{1,\alpha} = E''_{-1,\alpha}$.

For the homonuclear molecular ions the coupling between states of different g, u symmetry is zero and the above method is very good, but for $HD^+$ the results become worse (when compared with experiment) as the dissociation limit is approached. This is because the coupling between the $1s\sigma$ and $2p\sigma$ states increases at large internuclear distances and should no longer be treated as a perturbation. To overcome this problem Wolniewicz and Poll introduced the coupled zero-order wavefunction,

$$\psi^0 = \frac{1}{R}\left(\varphi_1^{\mathrm{BO}}(R, r_g)F_1^0(R) + \varphi_2^{\mathrm{BO}}(R, r_g)F_2^0(R)\right)Y_{NM}(\hat{R}) \tag{36}$$

where $\varphi_1$ and $\varphi_2$ are Born-Oppenheimer solutions of the $1s\sigma$ and $2p\sigma$ states respectively, $Y_{NM}(\hat{R})$ are spherical harmonics describing the rotation of the molecule and $F_1^0$ and $F_2^0$ satisfy a set of coupled equations which can be solved to give $F_{v,N}^0$ and $E_{v,N}^0$, to be used in place of $F^{\mathrm{ad}}$ and $E^{\mathrm{ad}}$ in the method outlined above. The non-adiabatic corrections $E''$ were tabulated for $HD^+$ vibrational levels $v = 0$–21, with rotational quantum states $N = 0, 3, 5$ for $\Sigma$-$\Sigma$ coupling and $N = 1, 3, 5$ for $\Sigma$-$\Pi$ coupling. The corrections were interpolated and extrapolated to other $N$ states using a least-squares fit.

Wolniewicz and Poll (1986) have tabulated the energy levels for $H_2^+$ $v = 0$–18, $N = 0$–5 and $HD^+$ $v = 0$–21, $N = 0$–8 in the electronic ground state. Radiative and relativistic corrections were included and give the most accurate set of energy levels published so far. Unfortunately they did not identify $v = 19$ or $v = 22$ as the highest bound levels in $H_2^+$ and $HD^+$, and their original eigenenergies quoted for $H_2^+$ were in error by the relativistic correction to the energy of a hydrogen atom, i.e. by 1.461 $\mathrm{cm}^{-1}$ (see the correction given by Wolniewicz and Poll (1989)).

### *2.7. The effect of an electric field.*

As will be described, the effect of a static electric field is crucial to much of our experimental work. The theory of the effect of an electric field upon the eigenvalues of the Hamiltonian has been considered by Hiskes (1961) and with more accuracy by Wind (1966). Hiskes chose to work within the centre of nuclear mass coordinate system, which is defined by the transformation (and its inverse),

$$\begin{bmatrix} r_c \\ R \\ R_{cm} \end{bmatrix} = \begin{bmatrix} -m_1/M_n & -m_2/M_n & 1 \\ -1 & 1 & 0 \\ m_1/M & m_2/M & m_e/M \end{bmatrix}\begin{bmatrix} r_1 \\ r_2 \\ r_e \end{bmatrix}$$

$$\begin{bmatrix} r_1 \\ r_2 \\ r_e \end{bmatrix} = \begin{bmatrix} -m_e/M & -m_2/M_n & 1 \\ -m_e/M & m_1/M_n & 0 \\ M_n/M & 0 & 1 \end{bmatrix}\begin{bmatrix} r_c \\ R \\ R_{cm} \end{bmatrix} \tag{37}$$

where $M = m_1 + m_2 + m_e$ and $M_n = m_1 + m_2$. The new vector $r_c$ is the position of the electron relative to the centre of nuclear mass. The inclusion of an electric field $\boldsymbol{F}$ into the Hamiltonian leads to an additional term $V_2$ in the potential energy, where

$$V_2 = -e\boldsymbol{F}\cdot(r_1 + r_2 - r_e). \tag{38}$$

Transformation of the Hamiltonian (1), including the new term $V_2$ to centre of nuclear mass coordinates gives (after removal of the centre-of-mass translation)

$$\frac{-\hbar^2}{2}\left[\frac{\nabla_c^2}{m_e} + \frac{\nabla_R^2}{\mu} + \frac{\nabla_c^2}{M_n}\right] + V + eF_z\left[\left(1 + \frac{m_e}{M}\right)z_c - \left(\frac{m_2 - m_1}{M_n}\right)z_R\right] \tag{39}$$

where the field has been fixed in the space-fixed $z$ direction and $z_c$ and $z_R$ are components of the $\boldsymbol{r}_c$ and $\boldsymbol{R}$ vectors. The first term involving the electric field describes its effect on the electron, whilst the second term describes its effect on the nuclei. For nuclei of equal mass the second term disappears as both nuclei are accelerated at the same rate. Applying the Born expansion (17), and neglecting terms coupling nuclear and electronic motion, the appropriate Born–Oppenheimer and adiabatic Hamiltonians are defined. The Hamiltonian for clamped nuclei, with the field in the direction of the internuclear axis is

$$\frac{-\hbar^2}{2m_e}\nabla_c^2 + eF_z z_c\left(1+\frac{m_e}{M}\right) + V. \tag{40}$$

Hiskes solved the Schrödinger equation with this Hamiltonian. The primary effect of the electric field term in the Hamiltonian is to produce coupling between the $1s\sigma_g$ and $2p\sigma_u$ states (represented by $\mathscr{H}'_{gu}$) which are degenerate at large internuclear distance. In $HD^+$ there is already a g, u mixing term in the Hamiltonian, $\mathscr{H}^0_{gu}$. Hiskes diagonalised the Hamiltonian for clamped nuclei, retaining only the submatrix for the two lowest electronic states, and obtained the eigenvalues of this submatrix (cf the coupled-states theory). For the homonuclear molecules this submatrix is

$$\begin{pmatrix} U_{1s\sigma_g}(R) & \mathscr{H}'_{gu}(R) \\ \mathscr{H}'_{gu}(R) & U_{2p\sigma_u}(R) \end{pmatrix}. \tag{41}$$

The diagonalisation of this matrix leads to the situation illustrated in figure 2. For large values of $\boldsymbol{R}$ the potential energy curves are given by

$$\begin{aligned} E(1s\sigma) &= U_{1s\sigma_g} - \tfrac{1}{2}e\boldsymbol{F}\cdot\boldsymbol{R}(1+m/M) \\ E(2p\sigma) &= U_{2p\sigma_u} + \tfrac{1}{2}e\boldsymbol{F}\cdot\boldsymbol{R}(1+m/M). \end{aligned} \tag{42}$$

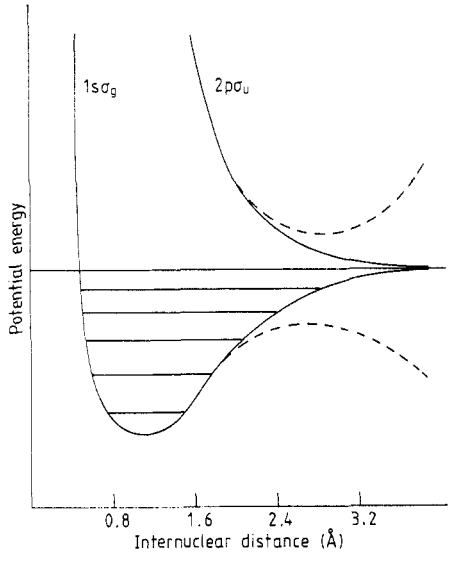


**Figure 2.** Potential energy curves for $H_2^+$. The full curves represent the unperturbed potentials, whilst the broken curves show the effect of an electric field applied along the internuclear axis. Vibrational levels are shown schematically, not to scale.

The increase in energy of the upper state is due to the clamped nuclei approximation; in the limit of large internuclear separation the ground electronic state corresponds to moving the free proton with the field, hence lowering the energy, and the first excited electronic state corresponds to moving the free proton against the field, hence raising the energy. Substitution of the potential curves into the radial Schrödinger equation allows the vibration-rotation levels and their lifetimes to be calculated. If the maximum of the potential is above an eigenvalue, then the molecule can predissociate by tunnelling. Hiskes calculated the electric fields required to dissociate $H_2^+$, finding that a field of $10^5$ V cm$^{-1}$ was sufficient to dissociate $v=18$, $N=0$ (dissociation energy 25.5 cm$^{-1}$) in $10^{-8}$ s. In the absence of tunnelling the molecule will dissociate 'classically' within one vibrational period (approximately $10^{-14}$ s) when the barrier height is lowered below the vibrational energy in the absence of a field. The fields required for 'classical' dissociation were calculated to be approximately twice those required for tunnelling in $10^{-8}$ s. In general it was found that for a given vibrational level, high-$N$ states required lower electric fields to dissociate at the same rate as low-$N$ states.

## 3. Nuclear hyperfine interactions

### *3.1. Derivation of the effective hyperfine Hamiltonian for $HD^+$*

The effects of the interactions between the electron and nuclear spins are represented in terms of an effective Hamiltonian which can be derived from the Dirac equation. For an electron interacting with an electromagnetic field described by the scalar and vector potentials, $\varphi$ and $\boldsymbol{A}$ respectively, the four-component wavefunction, $\Psi$, must satisfy the Dirac equation

$$\Psi = \{\beta m_e c^2 - e\varphi + c\boldsymbol{\alpha}\cdot\boldsymbol{\pi}\}\Psi \tag{43}$$

where $\boldsymbol{\alpha}$ and $\beta$ are Dirac matrices, and $\boldsymbol{\pi} = \boldsymbol{p} + e\boldsymbol{A}$ where $\boldsymbol{p}$ is the momentum of the electron. This equation may be converted into a non-relativistic form which has only positive energy solutions for a two-component wavefunction. A series of Foldy-Wouthuysen transformations are applied to equation (43), each transformation reducing the size of the odd operators which couple the positive and negative energy solutions. The fine-structure constant $\alpha = e^2\mu_0 c/2h$ is chosen as an expansion parameter, and after the application of three successive Foldy-Wouthuysen transformations (see, for example, Moss 1973) one obtains the following non-relativistic Hamiltonian, which is accurate to order $\alpha^6 mc^2$:

$$\mathscr{H} = m_e c^2 - e\varphi + \pi^2/2m_e \tag{44a}$$

$$+ g_e\mu_e(\boldsymbol{S}\cdot\boldsymbol{B}) - (g_e\mu_e/4m_e c^2)\boldsymbol{S}\cdot[\boldsymbol{\pi}\wedge\boldsymbol{E} - \boldsymbol{E}\wedge\boldsymbol{\pi}] \tag{44b}$$

$$+ (\hbar^2 e/8m_e^2 c^2)(\nabla\cdot\boldsymbol{E}) - (1/8m_e^3 c^2)\pi^4 - (g_e\mu_e/2m_e^2 c^2)(\boldsymbol{S}\cdot\boldsymbol{B})\pi^2. \tag{44c}$$

$\boldsymbol{S}$ is the electron spin angular momentum. The magnetic field, $\boldsymbol{B}$, and the electric field, $\boldsymbol{E}$, are related to the vector and scalar potentials by $\boldsymbol{B} = \nabla\wedge\boldsymbol{A}$ and $\boldsymbol{E} = -\nabla\varphi$. The vector potential, $\boldsymbol{A}$, at the electron is due to the magnetic moments of the nuclei. $m_e c^2$ is the rest energy of the electron and if $\boldsymbol{A}=0$ the other terms in (44$a$) give the non-relativistic electronic Hamiltonian discussed in the previous section. After further manipulation the first term in (44$b$) gives rise to the Fermi contact and dipole-dipole hyperfine interactions discussed below, and the second term is the spin-orbit coupling term, which for $\Sigma$ states is zero. The remaining terms (44$c$) are relativistic corrections.

An additional first-order term, the spin-rotation interaction due to the magnetic interaction between the rotating nuclei and the electron spin must be added. Collecting the various terms we obtain an effective first-order Hamiltonian for a particular value of the internuclear separation $R$

$$\mathcal{H}_{\text{eff}}(R) = b_1(R)\boldsymbol{I}_1 \cdot \boldsymbol{S} + b_2(R)\boldsymbol{I}_2 \cdot \boldsymbol{S} + c_1(R)I_{1z}S_z + c_2(R)I_{2z}S_z + \gamma(R)\boldsymbol{S} \cdot \boldsymbol{N}. \tag{45}$$

The subscripts 1 and 2 refer to the proton and deuteron in the $HD^+$ ion. Explicit expressions for the constants in (45) are given by Carrington and Kennedy (1985). A more convenient Hamiltonian is obtained by averaging over the appropriate radial wavefunction for any particular vibration-rotation level (see below), to yield

$$\mathcal{H}_{\text{eff}}(v, N) = b_1(v, N)\boldsymbol{I}_1 \cdot \boldsymbol{S} + b_2(v, N)\boldsymbol{I}_2 \cdot \boldsymbol{S} + c_1(v, N)I_{1z}S_z + c_2(v, N)I_{2z}S_z + \gamma(v, N)\boldsymbol{S} \cdot \boldsymbol{N}. \tag{46}$$

There are a number of second-order interactions which should also be included if a more accurate Hamiltonian is required (Dalgarno *et al* 1960). Although the hyperfine Hamiltonian (46) is in the well known form first presented by Frosch and Foley (1952), we prefer to use a rearranged form in which each term represents a different physical interaction. For $HD^+$ this is:

$$\mathcal{H}_{\text{eff}}(v, N) = b_{1\text{F}}(v, N)\boldsymbol{I}_1 \cdot \boldsymbol{S} + b_{2\text{F}}(v, N)\boldsymbol{I}_2 \cdot \boldsymbol{S} + t_1(2I_{1z}S_z - I_{1x}S_x - I_{1y}S_y) + t_2(2I_{2z}S_z - I_{2x}S_x - I_{2y}S_y) + \gamma\boldsymbol{S} \cdot \boldsymbol{N}. \tag{47}$$

The $b_{i\text{F}}$ constants in the first two terms now represent only the Fermi contact interactions, the $t_i$ constants are the axial components of the dipolar hyperfine interaction tensors, and $\gamma$ is, as before, the spin-rotation constant. The constants in (47) are related to those in (46) by the equations,

$$b_{i\text{F}} = b_i + \tfrac{1}{3}c_i \qquad t_i = \tfrac{1}{3}c_i. \tag{48}$$

The Fermi contact interaction for a particular value of the internuclear separation $R$ is given by

$$b_{i\text{F}}(R) = \frac{\mu_e \mu_n g_e g_{in}}{4\pi\varepsilon_0 c^2} \frac{8\pi}{3} \langle \delta(r_{ie}) \rangle \tag{49}$$

where $g_{in}$ is the nuclear $g$ constant and $r_{ie}$ is the distance between nucleus $i$, and the electron. The $\langle\ \rangle$ notation used refers to averaging over the electronic wavefunction, $\varphi_t(R)$. The Fermi contact constants for a particular vibration-rotation level (which appear in the effective Hamiltonian (47)) are then obtained by averaging over the radial wavefunctions $\chi_{vN}(R)$:

$$b_{i\text{F}}(v, N) = \int \chi_{vN}(R) b_{i\text{F}}(R) \chi_{vN}(R)\, \mathrm{d}R. \tag{50}$$

$\chi_{vN}$ is the solution of the radial Schrödinger equation (16), with an appropriate potential function. In a free hydrogen atom the proton Fermi contact constant, $b_{1\text{F}}$, has the value 1420.406 MHz whilst the deuteron Fermi contact interaction in a free deuterium atom is 218.05 MHz. It is informative to relate measured values of the Fermi contact constants in the molecular ions to these free atom values.

The first-order coupling of the electron spin ($\boldsymbol{S}$) with the rotation of the nuclei ($\boldsymbol{N}$) is given by

$$\gamma(R) = -\frac{\mu_e g_e e\hbar}{4\pi\varepsilon_0 c^2}[-\langle z_{1e}^3/Rr_{1e}\rangle(1/m_1) + \langle z_{2e}^3/Rr_{2e}\rangle(1/m_2)]. \tag{51}$$

Once again this must be averaged over the radial wavefunction to provide the $\gamma$ value appropriate for a particular $v,N$ level. The spin-rotation constants $\gamma(v, N)$ for $H_2^+$ and its deuterium isotopes are relatively small, particularly in the higher vibrational levels where the average internuclear distance is large. In heavier molecules and molecular ions the effective spin-rotation interaction is actually dominated by the second-order effects of spin-orbit coupling; in the hydrogen molecular ion, however, these second-order spin-orbit coupling effects are very small. Finally the dipolar constant $t_i$ is calculated for a given internuclear separation $R$ by evaluating the expression

$$t_i(R) = -\frac{\mu_e \mu_n g_e g_{in}}{4\pi\varepsilon_0 c^2}\langle (x_{ie}^2 - z_{ie}^2)/r_{ie}^5\rangle. \tag{52}$$

Integration over the radial wavefunction completes the determination for any particular $v, N$ level. The dipolar constants for $H_2^+$ and its isotopes are again relatively small, even in the lower vibrational levels, and become almost insignificant for the vibrational levels close to the dissociation limit.

There are other terms which might be required in the effective Hamiltonian if the spectroscopic resolution were high enough. In his work on the radiofrequency spectrum of $H_2^+$, for example, Jefferts (1968, 1969) found it necessary to include the term $f\boldsymbol{I}\cdot\boldsymbol{N}$, which represents the nuclear spin-rotation interaction. The $HD^+$ and $D_2^+$ ions could, in addition, show effects arising from the deuteron nuclear quadrupole interaction. This is, however, too small to be significant at our present level of resolution.

We have discussed the derivation of the hyperfine Hamiltonian for $HD^+$, which is the most complicated case in the present review. For the homonuclear molecules the hyperfine Hamiltonian takes a much simpler form; in $H_2^+$, for example, rotational levels in the ground electronic state which have even values of $N$ have net nuclear spin $I = 0$, so that only the spin-rotation term in the effective Hamiltonian (47) survives. Rotational levels with odd values of $N$ have $I = 1$, and the Fermi contact and axial dipolar interactions are each represented by a single term. $D_2^+$ has net nuclear spin $I = 1$ for odd-$N$ levels, and $I = 2$ and 0 for even-$N$ levels.

In all the vibration-rotation levels of $HD^+$ except those very close to the dissociation limit, we expect the largest hyperfine interaction to be the proton Fermi contact interaction. The deuteron Fermi contact constant is usually much smaller because of the smaller magnetogyric ratio of the deuterium nucleus. Consequently we choose the following basis set:

$$\begin{aligned} &\boldsymbol{G}_1 = \boldsymbol{S} + \boldsymbol{I}_1 && G_1 = 0; 1 \\ &\boldsymbol{G}_2 = \boldsymbol{G}_1 + \boldsymbol{I}_2 && G_2 = 1; 2, 1, 0 \\ &\boldsymbol{F} = \boldsymbol{G}_2 + \boldsymbol{N}. \end{aligned} \tag{53}$$

The matrix elements of the Hamiltonian (47) in this basis can be calculated using irreducible tensor methods. Calculation of the energies of the hyperfine components of any particular vibration-rotation level involves, at most, the diagonalisation of one $4\times4$ and two $3\times3$ matrices, which are tabulated by Carrington and Kennedy (1985).

Hyperfine energy level diagrams and the resulting hyperfine structure in the spectra are discussed in detail in the following sections.

## 4. Experimental methods

### *4.1. Electron impact ionisation of molecular hydrogen*

In all spectroscopic studies of $H_2^+$ and its deuterium isotopes the ions have been produced by electron impact ionisation of the neutral gas. We describe the ion source used in our experiments in § 4.3.2, but it is important to consider the ionisation process in some detail. Figure 3 shows the Born-Oppenheimer potential energy curves for HD and the ground and first excited electronic states of $HD^+$. These curves also apply to $H_2$ and $D_2$ and their cations. The neutral gas is introduced into the ion source which has an ambient temperature of approximately 500 K. Consequently all of the $H_2$ molecules are in the ground vibrational level ($v = 0$), with significant populations of only the first few rotational levels. Electron impact ionisation with electron energies in the range 50 to 100 eV is regarded as a vertical process to which the Franck-Condon principle may be applied. Since the potential energy curve for the $H_2^+$ ground state is relatively anharmonic and displaced to larger internuclear distances, all the vibrational levels of the ion are accessible through the vertical ionisation process and are therefore expected to be populated. If the ions are ejected into a high vacuum environment immediately after their formation, the initial vibrational populations are essentially preserved. Calculations of the Franck-Condon factors for ionisation have been carried out by a number of authors and the results are summarised in table 1. The quadrupole trap radiofrequency studies of Jefferts (1969) involved the $v = 4$ to 8 levels of $H_2^+$, whilst the vibration-rotation spectra of $HD^+$ described by Wing and his collaborators

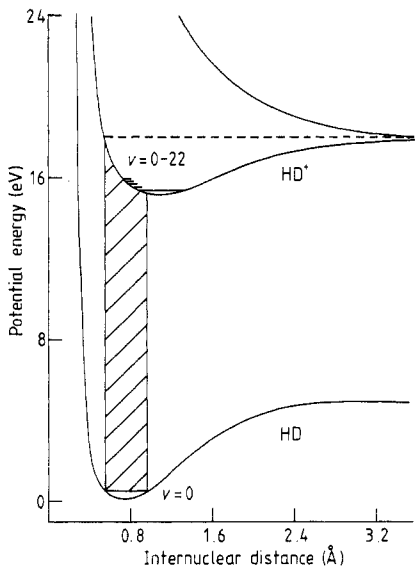


**Figure 3.** Born-Oppenheimer potential energy curves for HD and the ground and first excited electronic states of $HD^+$, illustrating vertical electron impact ionisation and the population of excited vibrational levels of $HD^+$.

**Table 1.** Vibrational populations of the $H_2^+$, $HD^+$ and $D_2^+$ ions resulting from electron impact ionisation of the neutral molecules (Dunn 1966, Tadjeddine and Parlant 1977). All three calculations use the Born-Oppenheimer potential for the ion. An asterisk denotes levels which are bound, but for which population factors have not been calculated.

| $v$ | $H_2^+$ | $HD^+$ | $D_2^+$ |
|---|---|---|---|
| 0 | 0.089 64 | 0.063 20 | 0.032 98 |
| 1 | 0.160 13 | 0.128 62 | 0.083 38 |
| 2 | 0.176 16 | 0.157 32 | 0.122 45 |
| 3 | 0.155 92 | 0.151 86 | 0.137 85 |
| 4 | 0.122 81 | 0.128 45 | 0.132 64 |
| 5 | 0.090 52 | 0.100 40 | 0.115 45 |
| 6 | 0.064 23 | 0.074 80 | 0.094 02 |
| 7 | 0.044 65 | 0.054 16 | 0.073 23 |
| 8 | 0.030 74 | 0.038 59 | 0.055 37 |
| 9 | 0.021 11 | 0.027 30 | 0.041 08 |
| 10 | 0.014 51 | 0.019 28 | 0.030 13 |
| 11 | 0.010 02 | 0.013 66 | 0.021 97 |
| 12 | 0.006 94 | 0.009 72 | 0.016 00 |
| 13 | 0.004 80 | 0.006 96 | 0.011 67 |
| 14 | 0.003 29 | 0.005 01 | 0.008 54 |
| 15 | 0.002 21 | 0.003 62 | 0.006 28 |
| 16 | 0.001 39 | 0.002 61 | 0.004 65 |
| 17 | 0.000 72 | 0.001 87 | 0.003 46 |
| 18 | 0.000 18 | 0.001 29 | 0.002 58 |
| 19 | * | 0.000 83 | 0.001 94 |
| 20 | | 0.000 45 | 0.001 45 |
| 21 | | 0.000 13 | 0.001 08 |
| 22 | | * | 0.000 78 |
| 23 | | | 0.000 54 |
| 24 | | | 0.000 34 |
| 25 | | | 0.000 16 |
| 26 | | | 0.000 04 |
| 27 | | | * |

(1976) were concerned with the $v = 0$ to 3 levels. Our infrared, microwave and radiofrequency studies of $HD^+$ involve the vibrational levels $v = 14$ to 22, the $v = 22$ level having been identified as the highest bound vibrational level in $HD^+$. The highest bound level in $D_2^+$ is calculated to be $v = 27$, and our work on this ion involves $v = 21$, 26 and 27 of the ground state. The populations of the high-lying vibrational levels produced by the initial ionisation process are crucial to the success of our experiments.

Provided the gas pressure in the ion source is sufficiently low, there is good reason to suppose that the vibrational populations in $HD^+$ given in table 1 are fairly accurate, with the further conclusion that the ionisation process does not produce rotational excitation. However, we employ relatively high source pressures in most of our work and as the source pressure is increased it appears that the populations of high-$v$ and high-$N$ levels in the diatomic ions are increased. As we describe later, we have observed a vibration-rotation transition in $HD^+$ which involves $N = 18$, and even higher $N$ levels are almost certainly populated. The origin of this internal excitation is not properly understood, but it might involve the formation and destruction of triatomic ions in the source, namely $H_3^+$ and its deuterium isotopes. Further increases in source pressure result in total conversion of the diatomic ions to triatomic. Consequently the

success and optimisation of our studies of the high vibrational levels of $HD^+$ depends crucially on the choice of the ion source pressure.

### *4.2. Quadrupole trap radiofrequency studies of $H_2^+$*

Dehmelt and Jefferts (1962) demonstrated that partial alignment of $H_2^+$ ions may be achieved by photodissociation with polarised white light. They used a pulse sequence in which $H_2^+$ ions were produced by an electron pulse and held in a quadrupole radiofrequency trap. The ions were irradiated continuously with polarised light from an arc lamp, in the presence of a weak magnetic field aligned parallel to the electric vector of the light. Figure 4(*a*) illustrates the hyperfine structure of $H_2^+$ in its $N = 1$ rotational level. The Fermi contact and dipolar hyperfine interactions produce a doublet splitting of the $F_2 = \frac{3}{2}$ and $\frac{1}{2}$ states. These are further split by the spin–rotation interaction, and the spatial degeneracy of each $F$ state is then removed by the applied magnetic field. Optical excitation to the repulsive $2p\sigma_u$ state results in photodissociation, but different $F$, $|M_F|$ components have different photodissociation rate factors ($R$) which are also shown in the figure. Consequently the relative populations of the different $F$, $M_F$ states of the remaining undissociated $H_2^+$ ions change as photodissociation proceeds. In other words, the undissociated $H_2^+$ ions develop a partial preferred spatial alignment, and this alignment is monitored by counting the number of photofragment $H^+$ ions produced during a certain time interval. If the direction of the magnetic field is then switched through 90°, the molecular alignment is partially destroyed and consequently the photodissociation rate is changed. Molecular alignment was therefore demonstrated by measuring the change in photodissociation rate with change in the magnetic field direction.

Richardson *et al* (1968) subsequently demonstrated that partial destruction of the photoinduced alignment can also be achieved by driving radiofrequency transitions between the magnetic sublevels shown in figure 4(*a*); the radiofrequency magnetic resonance spectrum was therefore recorded by monitoring the photodissociation rate and recording an increase when the magnetic resonance transitions were driven. In

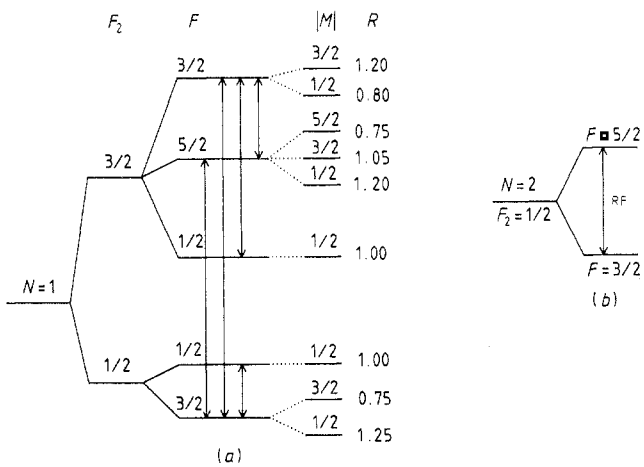


**Figure 4.** (*a*) Proton hyperfine, spin-rotation and Zeeman splitting of the $N = 1$ rotational levels of $H_2^+$, and observed radiofrequency transitions. (*b*) Spin-rotation splitting of the $N = 2$ rotational levels of $H_2^+$, and observed radiofrequency transition.

later work Jefferts (1968, 1969) was able to observe hyperfine transitions in the $N = 1$ and 2 rotational components of the $v = 4$–8 levels of $H_2^+$. Linewidths of 200 to 750 Hz were obtained so that the constants describing the proton Fermi contact interaction ($b_F$), electron-nuclear dipolar interaction ($t$), electron-spin-nuclear-rotation interaction ($\gamma$) and nuclear-spin-nuclear-rotation interaction ($f$) were determined very accurately (see table 4). The high spectroscopic resolution achieved in these experiments is a consequence of the long residence time of the ions in the radiation field applied to the ion trap. The spectroscopic sensitivity is not high, however, and these techniques have not been applied to the deuterium isotopes of $H_2^+$, or to any other molecular ions.

### *4.3. Infrared spectra of $HD^+$*

*4.3.1. General description of ion beam machines.* Wing *et al* (1976) in their pioneering studies of the $HD^+$ ion used an ion beam instrument which is shown schematically in figure 5. The ion beam is accelerated to a potential of a few kV, interacts with a carbon monoxide infrared laser beam (introduced at a small angle to the ion beam), passes through a gas collision cell, and is measured with a final Faraday cup detector. Ion currects of 0.1 $\mu$A are obtained. Vibration-rotation transitions are observed by using Doppler tuning (see § 4.3.3) and are detected as changes in $HD^+$ ion current at the Faraday cup. The laser beam is mechanically chopped at 1 kHz, so that the infrared resonances can be detected with a lock-in amplifier. The principles underlying the detection of the resonances, and the experimental results, are described in § 4.3.4 and table 2.

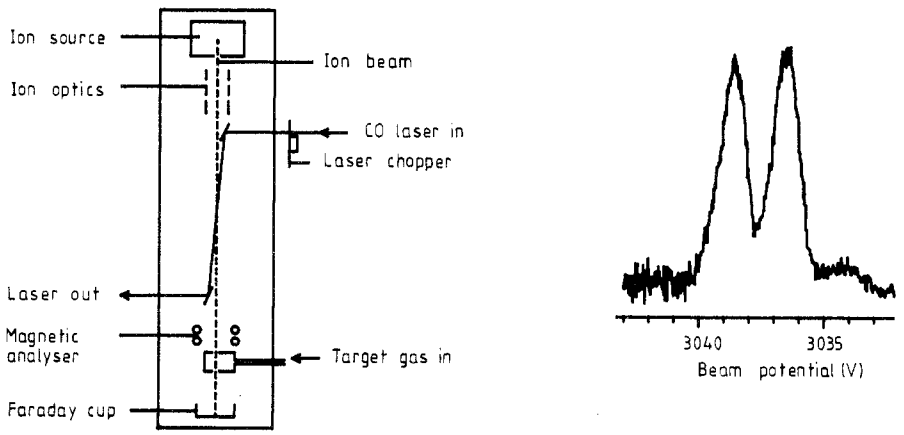


**Figure 5.** Ion beam machine used by Wing *et al* (1976) in their studies of the $HD^+$ ion, and a recording of the 1,1-0,2 vibration-rotation transition showing nuclear hyperfine structure.

We have employed two different ion beam machines for the work described in this review. The first is a modified Vacuum Generators ZAB 1F tandem mass spectrometer, the main features of which are illustrated in figure 6($a$). The ions are formed by electron impact and are accelerated to a maximum potential of +10 kV. The ion beam is focused into a 55°, 30 cm radius magnetic sector and may then be detected by means of an off-axis electron multiplier. By scanning either the ion source potential or the

**Table 2.** Experimental and theoretical vibration–rotation frequencies for $HD^+$.

| Transition | | Expt | Born–Opp | Standard adiabatic | Coupled states | Non-adiabatic |
|---|---|---|---|---|---|---|
| 1–0 | P(1) | 1869.134 | 1869.722 | 1869.262 | 1869.262 | 1869.131 |
| | P(2) | 1823.533 | 1824.101 | 1823.660 | 1823.660 | 1823.530 |
| | P(3) | 1776.459 | 1777.006 | 1776.585 | 1776.585 | 1776.456 |
| 2–1 | R(0) | 1856.778 | 1857.331 | 1856.898 | 1856.898 | 1856.778 |
| 3–2 | R(0) | 1761.616 | 1762.100 | 1761.727 | 1761.727 | 1761.616 |
| | R(1) | 1797.522 | 1798.018 | 1797.634 | 1797.634 | 1797.522 |
| | R(2) | 1831.083 | 1831.589 | 1831.194 | 1831.194 | 1831.083 |
| | P(2) | 1642.108 | 1642.545 | 1642.216 | 1642.216 | 1642.107 |
| 17–14 | R(0) | 1813.852 | 1812.510 | 1813.684 | 1813.640 | 1813.857 |
| | R(1) | 1820.209 | 1818.848 | 1820.035 | 1819.990 | 1820.212 |
| | R(2) | 1820.199 | 1818.816 | 1820.022 | 1819.976 | 1820.203 |
| | R(3) | 1813.644 | 1812.231 | 1813.463 | 1813.415 | 1813.649 |
| | R(4) | 1800.358 | 1798.906 | 1800.171 | 1800.120 | 1800.362 |
| | R(5) | 1780.145 | 1778.648 | 1779.951 | 1779.896 | 1780.149 |
| | P(1) | 1782.772 | 1781.443 | 1782.606 | 1782.563 | 1782.776 |
| 17–15 | R(7) | 1078.853 | 1077.661 | 1078.691 | 1078.633 | 1078.856 |
| | P(1) | 1092.124 | 1091.159 | 1091.993 | 1091.959 | 1092.125 |
| | P(2) | 1071.561 | 1070.596 | 1071.432 | 1071.397 | 1071.563 |
| | P(3) | 1047.239 | 1046.271 | 1047.108 | 1047.073 | 1047.241 |
| | P(5) | 987.917 | 986.930 | 987.786 | 987.747 | 987.919 |
| | P(6) | 953.180 | 952.178 | 953.048 | 953.007 | 953.184 |
| 18–16 | R(0) | 926.490 | 925.351 | 926.333 | 926.263 | 926.494 |
| | R(1) | 932.224 | 931.068 | 932.065 | 931.993 | 932.228 |
| | R(2) | 933.213 | 932.036 | 933.052 | 932.976 | 933.217 |
| | R(3) | 929.247 | 928.044 | 929.084 | 929.004 | 929.252 |
| | R(4) | 920.100 | 918.865 | 919.936 | 919.846 | 920.104 |
| | R(5) | 905.519 | 904.248 | 905.356 | 905.256 | 905.525 |
| | R(6) | 885.218 | 883.906 | 885.058 | 884.943 | 885.224 |
| | P(1) | 901.565 | 900.445 | 901.411 | 901.343 | 901.568 |
| | P(2) | 882.731 | 881.617 | 882.581 | 882.512 | 882.736 |
| 20–17 | R(0) | 918.102 | 916.633 | 918.418 | 917.946 | 918.111 |
| | R(1) | 915.476 | 914.051 | 915.861 | 915.358 | 915.486 |
| | R(2) | 904.833 | 903.598 | 905.345 | 904.780 | 904.845 |
| | R(3) | 885.749 | 884.593 | 886.447 | 885.798 | 885.767 |
| | P(1) | 900.488 | 899.016 | 900.776 | 900.319 | 900.496 |
| | P(2) | 880.668 | 879.228 | 880.989 | 880.519 | 880.675 |
| 21–17 | R(0) | 998.533 | 1003.715 | 1006.152 | 998.849 | 998.536 |
| | R(1) | 988.993 | 995.235 | 997.699 | 989.161 | 988.991 |
| | R(2) | 967.811 | 975.688 | 978.191 | 967.694 | 967.833 |
| | P(1) | 984.330 | 989.023 | 911.433 | 984.715 | 984.341 |
| | P(3) | 927.192 | 933.484 | 935.908 | 927.373 | 927.190 |
| | P(4) | 882.523 | 890.474 | 892.918 | 882.426 | 882.547 |
| 22–17 | R(0) | 1006.965 | 1018.074 | 1020.762 | 1006.227 | † |
| | P(1) | 994.112 | 1005.126 | 1007.798 | 993.426 | † |
| | P(2) | 969.530 | 980.669 | 983.333 | 968.800 | † |

† Transitions to $v = 22$ levels whose non-adiabatic energies were not calculated.

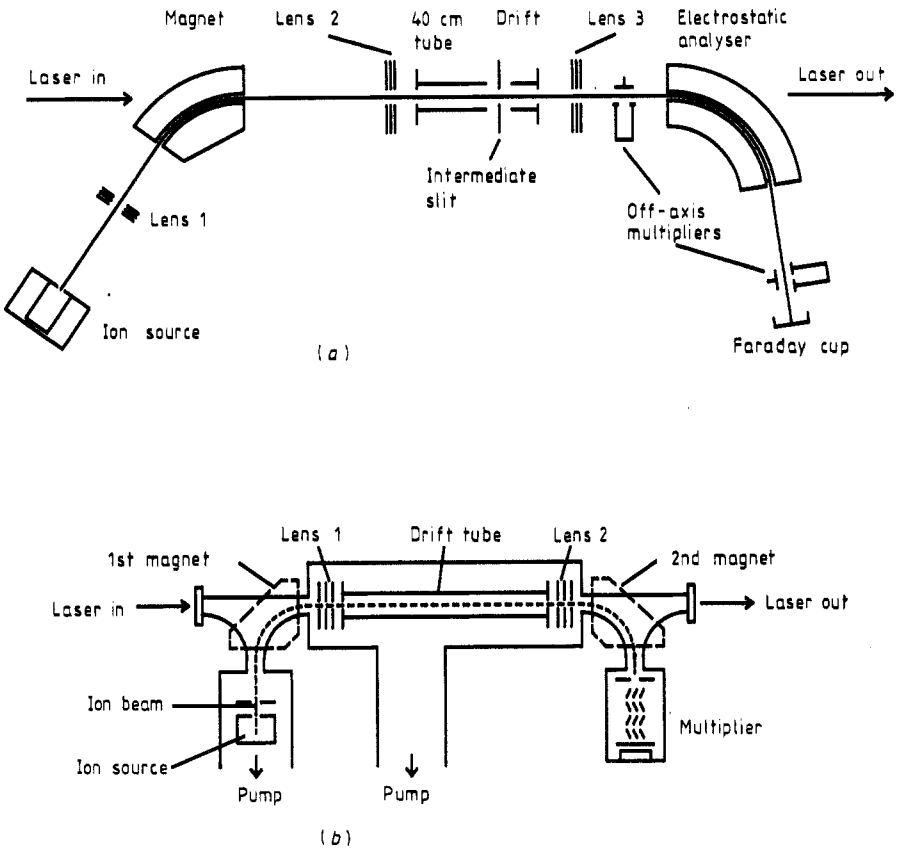


**Figure 6.** (*a*) Block diagram of the ZAB tandem mass spectrometer used in studies of the vibration-rotation spectrum of the $HD^+$ ion, detected by monitoring photofragment ions. (*b*) Block diagram of the ion beam machine (NIB) as used in studies of the infrared spectra of $HD^+$, with detection by photodissociation.

magnet current, the single focus mass spectrum of the source gas may be recorded, and the magnet current then set to transmit the desired ion beam.

The ion beam traverses a field-free region before entering a metal tube of length 40 cm and diameter 2 cm, which we call the drift tube. Towards the end of this tube the ion beam reaches a focus at the intermediate slit, after which it is transmitted through an electrostatic analyser (ESA) of 38 cm radius. Following the ESA the beam is detected either with a second off-axis electron multiplier, or with a Faraday cup. The ion beam pathlength from source to detector is 2.5 m. Our normal mode of operation in the spectroscopic experiments is to use the magnetic sector to select the required parent ions (for example, $HD^+$), and the ESA to separate the desired fragment ions ($H^+$ or $D^+$). The geometry of the apparatus allows a clear axial line of sight, although it is necessary to drill a small hole through the ESA for this purpose. It is therefore easy to bring an infrared laser beam through zinc selenide windows and into coincidence with the ion beam between the two sectors, and for photofragment ions to be separated by means of the ESA.

The drift tube serves two important purposes in our experiments. Application of an auxiliary positive or negative potential (500 V maximum) to the drift tube means

that the parent ion beam is either retarded or accelerated on entering the tube. Consequently fragment ions formed inside the drift tube and re-accelerated on exit have a different kinetic energy from those formed outside, and may be separated with the ESA; we usually choose to monitor those fragments formed inside the drift tube. As we describe in the following section, the drift tube is also used for modulation purposes.

Our second and newer ion beam machine (NIB, shown in figure 6(*b*)) is also a tandem mass spectrometer, but differs in many important respects from the ZAB. It employs two 90°, 6 cm radius magnetic sectors and the ion beam path from the source to the detector is only 1.0 m. The instrument incorporates two identical lens stacks which provide focusing and deflection of the ion beam; the first lens stack is placed immediately after the first magnet, and the second lens assembly is situated just before the second magnet. The final detector is an axial electron multiplier, but beam monitor plates which intersect a small portion of the ion beam are placed in both lens stacks, and also after the second magnet. Interaction of the ion and laser beams occurs in the region between the two lens assemblies, and we have inserted a number of devices in this region of the machine, depending upon the type of spectroscopic study required. For the infrared vibration–rotation studies we use a metal drift tube of length 26 cm. In other work, described later, we have used radiofrequency or microwave cells, and we have also included an electric field dissociation lens prior to the second focusing lens stack.

The infrared radiation source used in most of our work with both ion beam machines has been a CW carbon dioxide infrared laser, although a few studies have employed a carbon monoxide laser. We use Edinburgh Instruments PL3 or PL4 lasers. The PL4 laser operated in a flowing gas mode with $^{12}CO_2$ provides output powers of up to 50 W, and with $^{13}CO_2$ as the lasing medium, sealed-mode operation gives powers up to a maximum of 20 W. The lasers use rotatable gratings to provide laser line selection, and the use of both carbon isotopes provides laser lines covering the region from 874 to 1094 $cm^{-1}$. Coarse spectroscopic scanning is accomplished by selecting different laser lines, whilst the fine tuning utilises the Doppler effect, as described in § 4.3.3.

*4.3.2. Ion source.* In our experiments the ions are formed by electron impact ionisation, an electron beam being produced by means of a heated tungsten wire filament which is held at potentials of −20 to −110 V with respect to the source body. The electron beam is confined by means of two small permanent magnets and, after passage through the source, is collected with a metal trap, where electron currents of up to 1 mA are measured. Electronic stabilisation circuitry is employed to control the filament current so that a constant electron beam trap current is obtained. The neutral gas is introduced into the source through a small inlet hole and escapes through the electron and ion slits. The ion source is therefore relatively gas tight, and with $H_2$ as the source gas the pressure outside the source is typically $5 \times 10^{-6}$ mbar when the maximum $H_2^+$ beam intensity is obtained. We estimate the pressure inside the source to be in the range $10^{-3}$ to $10^{-4}$ mbar. $HD^+$ beams are obtained by passing an equal mixture of $H_2$ and $D_2$ over a heated palladium catalyst to form HD gas prior to entry into the ion source.

In the ZAB instrument the ion source potential may be tuned to a maximum of +10 kV, with the remainder of the machine being at earth potential. In the NIB instrument we have had a maximum source potential of +5 kV available, although this has recently been increased to +10 kV. The positive molecular (and atomic) ions are accelerated through an ion exit slit of width 1 mm and length 5 mm to form a beam

with a rectangular cross section. An ion repeller plate is placed inside the ion source, and small auxiliary potentials may be applied to this to maximise the efficiency of ion extraction. In both instruments the $H_2^+$ beam current measured just outside the source is a few $\mu$A at a beam potential of 5 kV. After transmission through two magnetic sectors, or one magnetic and one electrostatic sector, the maximum final $H_2^+$ beam current is 1 $\mu$A.

*4.3.3. Doppler tuning and modulation.* The velocity of the molecular ions in the beam ($v$) depends upon their charge ($q$), mass ($m$) and acceleration potential ($V$), according to the equation

$$\tfrac{1}{2}mv^2 = qV. \tag{54}$$

For the $HD^+$ ion at a beam potential of 5 kV the ion velocity is $5.7 \times 10^5$ m s$^{-1}$, and since the laser beam is aligned to be collinear and coincident with the ion beam, there is a large Doppler shift. The apparent radiation frequency experienced by the molecules ($\nu_{\text{ion}}$) is proportional to the actual laser frequency ($\nu_{\text{laser}}$) according to the relativistic formula

$$\nu_{\text{ion}} = \nu_{\text{laser}}\{[1 \mp (v/c)]/[1 \pm (v/c)]\}^{1/2} \tag{55}$$

where the upper signs are for parallel propagation and the lower signs for antiparallel propagation of the ion and laser beams. For a laser wavenumber of 1000 cm$^{-1}$ and $HD^+$ ion beam potentials of 1 and 10 kV, the Doppler shifts are $\pm 0.85$ and $\pm 2.68$ cm$^{-1}$ respectively. In the carbon dioxide infrared laser the laser lines are spaced at 1 to 2 cm$^{-1}$, except for the larger gaps between band systems, so that Doppler scanning is easy and convenient, particularly for light ions such as those discussed in this review. In the ZAB instrument we scan the ion source potential, with synchronous computer-controlled scanning of the magnetic and electric sectors so that the fragment ion current at the final electron multiplier is monitored continuously. In the NIB instrument Doppler scanning voltages are applied only to the drift tube located between the magnetic sectors.

In order to calibrate spectra in wavenumber units it is, of course, necessary to have a precise measure of the ion beam potential. This is not quite the same as the voltage potential applied to the ion source, because of earth field penetration into the source, and the effects of any repeller plate potential. The true ion beam potential is therefore different from the applied potential, but an appropriate correction factor can be accurately determined by measuring the same spectroscopic line (in $HD^+$, for example) using two different laser lines aligned parallel and antiparallel with the ion beam. We found the correction factor for the 5 kV source of the NIB instrument to be 0.994.

In both instruments we find it convenient to use the Doppler shift for modulation purposes in detecting spectroscopic lines. Application of an oscillating voltage (typically up to a maximum of 10 V at 10 kHz) to the drift tube results in velocity modulation of the ion beam and hence, through the Doppler effect, to frequency modulation. Spectroscopic absorption lines are therefore measured by using a lock-in amplifier to detect the AC output from the electron multiplier detector, which is referenced at the Doppler modulation frequency. Drift tube modulation is, in general, more satisfactory than laser chopping because in most cases there is a non-resonant photofragment background.

Another important effect which arises from the high molecular velocities obtained by accelerating ion beams is kinematic compression, or velocity bunching (Kaufman 1976). The ions in the beam possess a spread of laboratory energies, perhaps as large

as 1.5 eV, because of potential inhomogeneities inside the ion source. Fortunately the Doppler width is determined by the ratio of the velocity spread to the absolute velocity in the beam, and this ratio becomes progressively smaller as the ion beam potential (and hence the molecular velocity) is increased. The Doppler width is therefore reduced, and for a light ion like $HD^+$ at a beam potential of 8 kV, the kinematic reduction in the Doppler width is a factor of 200. The result is that at $\nu = 1000\ cm^{-1}$ the Doppler width for $HD^+$ is about 5 MHz. Ion beam spectroscopy is therefore capable of much higher resolution than is normally obtained with molecules which are, on average, at rest in the laboratory frame of reference.

*4.3.4. Spectroscopic detection by charge exchange.* We have already noted that Wing and his collaborators introduced a gas collision cell into their apparatus as the means of detecting vibration-rotation transitions. The $HD^+$ ion current detected at the Faraday cup (see figure 5) is reduced by collisions with the collision gas, usually hydrogen, primarily because of charge exchange. The $H_2^+$ ions produced by the charge-exchange reaction are not in the ion beam, so that the beam intensity is reduced, even though the total number of ions is not affected. The charge-exchange reaction may be used as the basis for detecting spectroscopic excitation of the $HD^+$ ions, provided the charge-exchange cross section changes sufficiently with a change in the internal vibration-rotation state of the $HD^+$ ions. For transitions involving $v = 0$ to 3 and $N = 0$ to 3, changes of approximately $3 \times 10^{-6}$ in the total $HD^+$ beam current were observed. The resulting signals were measured against the statistical noise of the full parent beam, and signal-to-noise ratios of 2:1 were observed using laser chopping and phase-sensitive detection with a 1 s averaging time. The success of these experiments also depends upon there being a large enough population difference between the two levels involved before laser excitation, and upon efficient population transfer induced by the laser on resonance.

Figure 5 shows a typical vibration-rotation transition, exhibiting nuclear hyperfine structure. The wavenumbers of eight vibration-rotation transitions were measured with an accuracy of $0.001\ cm^{-1}$, and the results are considered in more detail in § 4.3.8.

*4.3.5. Spectroscopic detection by photodissociation.* Since all of the bound vibrational levels of $HD^+$ ($v = 0$ to 22) are populated in an ion beam, one expects to observe photodissociation, even with an infrared radiation source. This is because the first excited electronic state ($2p\sigma$) is almost wholly repulsive, and becomes nearly degenerate with the $1s\sigma$ ground state at the dissociation limit. The ion beam instruments illustrated in figures 6(*a*) and 6(*b*) are ideal for studying photodissociation, since the photofragment ions can be separated from the parent ions by the second sector. Carrington *et al* (1988a) have used the ZAB, combined with perpendicular laser beam irradiation, to measure the relative photodissociation cross sections for $H_2^+$, $D_2^+$ and $HD^+$ in the infrared region spanned by the carbon dioxide laser; the ESA was used to separate fragment ions with different kinetic energies arising from different vibrational levels. $HD^+$ ions in $v = 18$ have the largest photodissociation cross section at $1000 \pm 100\ cm^{-1}$, but ions in $v = 19$–21 also photodissociate significantly.

This photodissociation can be used as the basis for detecting vibration-rotation transitions (Carrington *et al* 1979, Carrington and Buttenshaw 1981); the principles are illustrated in figure 7. $HD^+$ ions in, for example, $v = 16$ lie too far below the repulsive state to be dissociated by absorption of a single infrared photon, but they may be excited to rotational components of $v = 18$, and thence to the repulsive state

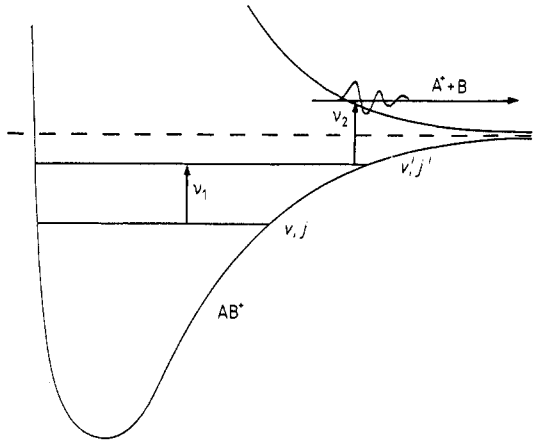


**Figure 7.** Principles involved in the detection of vibration-rotation transitions in $HD^+$ by photodissociation. $\nu_1$ is a transition between bound vibration-rotation levels in the ground state, and $\nu_2$ is an electronic transition to the repulsive excited electronic state which undergoes rapid photodissociation.

by subsequent absorption of a second photon. Vibration-rotation transitions are therefore detected by monitoring the increased photofragment ion yield on resonance. Deuterons or protons may be monitored, but we usually choose to observe the deuterons because of their greater mass. The experiments have been performed using a single laser to provide both photons, or two differerent lasers oriented parallel and antiparallel to the ion beam. In the latter case we have carried out experiments using either two carbon dioxide lasers, or one carbon dioxide and one carbon monoxide laser (Carrington *et al* 1983).

The photodissociation method is more sensitive than charge exchange because the noise arises only from the photofragment background, and not the full parent ion beam. The sensitivity depends, however, on the photodissociation cross section for the upper level in the vibration-rotation transition. Since ions in $v = 18$ have the largest photodissociation cross sections in the carbon dioxide laser region, photodissociation is a particularly sensitive method for studying rotational components of the 18-16 band. The sensitivity for studying the 21-17 band is very much lower, however, partly because the photodissociation cross section for $v = 21$ is small, and partly because the signal must be detected against the large non-resonant photofragment background arising from ions in $v = 18$. An example of a spectrum requiring three hours of signal averaging (Carrington *et al* 1987, 1988b) is shown in figure 8(*a*). Nevertheless we have used the photodissociation method to study vibrational band systems in $HD^+$ involving $v = 14$ to 21, and the results are discussed in § 4.3.8.

*4.3.6. Rotational predissociation.* The potential energy curves for states with large rotational angular momentum ($N$) exhibit maxima because of the centrifugal energy, and therefore approach the dissociation limit asymptotically from higher energies. Consequently it is possible to find vibrational levels which lie above the dissociation limit, but below the centrifugal barrier maximum, so that they are metastable. Carrington *et al* (1988c) have observed the vibration-rotation transition 16,17-13,18, the 16,17 level being rotationally quasibound with a lifetime of $10^{-8}$ s. Figure 9 shows the potential curves for $N = 17$, and indicates the observed bound to quasibound

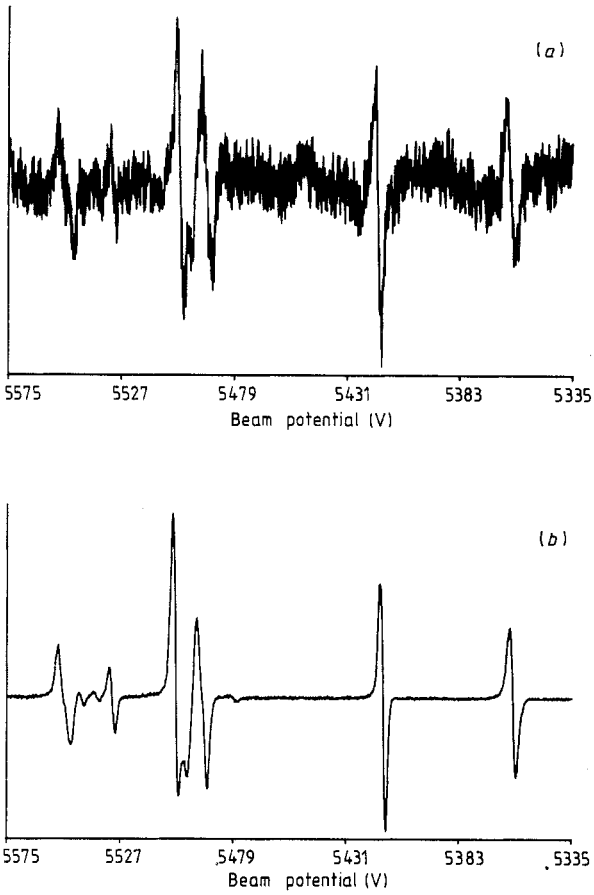


**Figure 8.** (*a*) Recording of the 21,2-17,3 vibration-rotation transition in $HD^+$, detected by measuring $D^+$ fragment ions produced by photodissociation. (*b*) Recording of the 21,2-17,3 vibration-rotation transition in $HD^+$, detected by measuring $H^+$ fragment ions produced by electric field dissociation of the 21,2 level.

transition. The vibration-rotation line can only be detected by monitoring fragment protons, which result from tunnelling through the centrifugal barrier. This is in contrast to the detection of bound-to-bound transitions by subsequent photodissociation, which can be achieved by monitoring either protons or deuterons. For the bound to quasi-bound transition we remain on the ground-state potential curve, which correlates with the $H^+ + D$ dissociation limit. The width of the observed line is determined by the predissociation lifetime; experiment and theory are in excellent agreement.

*4.3.7. Electric field dissociation.* Riviere and Sweetman (1960) and Wind (1964) showed that $H_2^+$ ions can be dissociated by an electric field, and Bjerre and Keiding (1986) have used electric field dissociation to detect laser-induced electronic excitation in $O_2^+$ ions. We have recently incorporated an electric field dissociation lens in the small ion beam machine, as shown in figure 11 (Carrington *et al* 1988d). An $HD^+$ ion beam passes first through the drift tube for Doppler tuning into resonance with the laser beam, and then through a four-plate structure in which a positive potential is applied

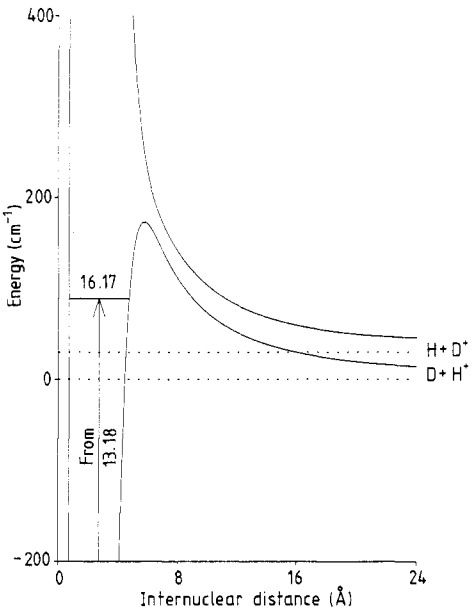


**Figure 9.** Potential energy curves for the $N = 17$ rotational level of $HD^+$, showing the bound to quasibound transition and the correlation of the electronic states with the separated dissociation limits.

to the inner pair of plates as shown. Electric fields from $10^2$ to $10^4$ V cm$^{-1}$ have been used in our work.

Consideration of the ground-state potential energy curve of $HD^+$ shows that the addition of an electric field depresses the energy of the $H^+ + D$ dissociation limit, so that vibration-rotation levels which are bound in zero electric field become unbound or quasibound in the presence of the field. In our experiments it seems clear that the ions predissociate by tunnelling through the field-induced barrier, with a lifetime depending on the zero-field dissociation energy of the vibration-rotation level and the strength of the applied electric field. The result is that protons formed in the lens have a characteristic momentum which is usually different from that of the background protons, and they may therefore be separated by means of the magnetic analyser. Figure 8 compares spectra obtained by photodissociation and electric field dissociation; in the most favourable cases the sensitivity using electric fields is enhanced by four orders of magnitude. The nuclear hyperfine structure of the 21-17 and 22-17 transitions is cleanly resolved, and will be discussed in more detail in § 4.3.9.

*4.3.8. Comparison of experimental and theoretical vibration-rotation frequencies.* In table 2 we have summarised all of the experimentally determined vibration-rotation frequencies for $HD^+$, and compared them with theoretical predictions. The first comparison is with the results of Born-Oppenheimer calculations, and we see that although the theory is fairly satisfactory for transitions involving the lower vibrational levels, it becomes grossly inaccurate as we approach the dissociation limit. The adiabatic and coupled-state results of Kennedy are shown next, and finally we compare the experimental results with the predictions from the non-adiabatic calculations of Wolniewicz and Poll (1986), which also include relativistic and radiative corrections. The agreement between experiment and the most complete theoretical calculations

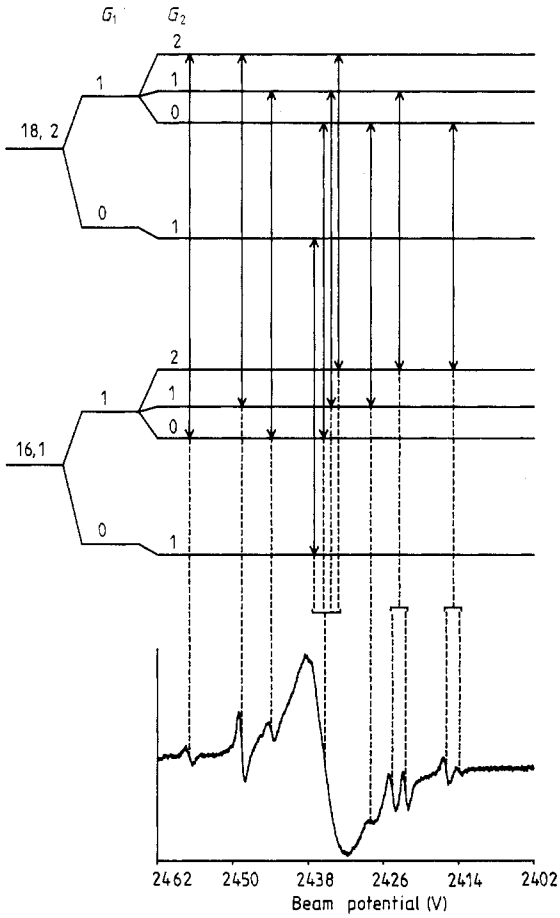


**Figure 10.** Nuclear hyperfine splitting of the 18,2 and 16,1 vibration-rotation levels of $HD^+$, showing the correlation of the allowed and forbidden transitions with the observed spectrum.

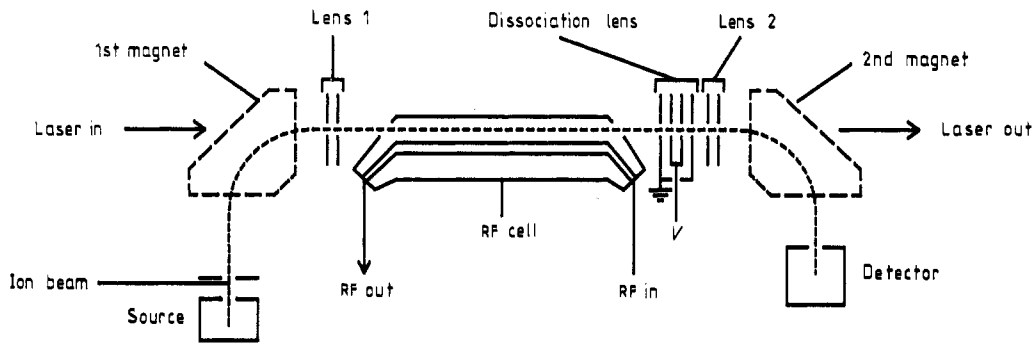


**Figure 11.** Block diagram of the ion beam machine used in the study of radiofrequency/infrared double resonance transitions in $HD^+$, illustrating the electric field dissociation lens.

provides a convincing demonstration of the reliability and power of molecular quantum mechanics. A further conclusion to be drawn from these comparisons is that Born-Oppenheimer calculations for more complex systems, particularly in high-energy states, might be seriously inaccurate because of the neglect of adiabatic and non-adiabatic effects, quite apart from the problems arising from electron correlation and relativistic effects.

*4.3.9. Nuclear hyperfine structure.* We discussed the theory of the nuclear hyperfine structure in § 3, and showed that, for $HD^+$, the effective hyperfine Hamiltonian may be written in the form (47),

$$\mathcal{H}_{\text{eff}} = b_{1\text{F}}\boldsymbol{S}\,.\,\boldsymbol{I}_1 + b_{2\text{F}}\boldsymbol{S}\,.\,\boldsymbol{I}_2 + t_1(2S_zI_{1z} - S_xI_{1x} - S_yI_{1y}) + t_2(2S_zI_{2z} - S_xI_{2x} - S_yI_{2y}) + \gamma\boldsymbol{S}\cdot\boldsymbol{N}.$$

$b_{1\text{F}}$ and $b_{2\text{F}}$ are the Fermi contact hyperfine constants for the proton and deuteron nuclei, $t_1$ and $t_2$ are the axial components of the dipolar hyperfine tensors, and $\gamma$ is the spin-rotation constant. This Hamiltonian is adequate to describe the nuclear hyperfine structure in the infrared spectra, but for spectra of higher resolution further terms might need to be included.

Theoretical values of the hyperfine constants have been listed by Carrington and Kennedy (1985) and Kennedy *et al* (1988) using the coupled-states theory. For vibration-rotation levels which lie well below the dissociation limit, one expects $b_{1\text{F}}$ and $b_{2\text{F}}$ to have values close to half their free atom values (1420.41 and 218.05 MHz), since the electron should be shared equally between the two nuclei. In the lowest vibrational levels the observed and calculated values are larger because the $He^+$ united-atom limit is approached, but in the high-lying levels we have studied, half the free-atom value should be a good estimate of $b_{1\text{F}}$ and $b_{2\text{F}}$, provided the electron distribution is symmetric. The dipolar and spin-rotation constants are likely to become very small as we approach the dissociation limit, because the average internuclear separation becomes very large.

The best basis for describing the coupling of the various angular momenta in $HD^+$ is that given in (53). The hyperfine splitting for 18,2 and 16,1 is shown in figure 10. The four central electric dipole vibration-rotation transitions indicated in the figure are diagonal in $G_1$ and $G_2$, and since the hyperfine splittings in the lower and upper states are very similar, the main infrared line shows little or no hyperfine structure. Consequently it is difficult to determine the hyperfine constants from the infrared vibration-rotation spectra, because the transitions which are off-diagonal in $G_1$ or $G_2$, which would provide hyperfine information, are very weak. Physically this problem arises because of the very small spin-rotation interaction. The electron spin is only very weakly coupled to the orientation of the electric dipole moment (which is along the internuclear axis), so that transitions which involve a change in the nuclear spin orientation have very little electric dipole intensity. Despite these problems Carrington *et al* (1988e) were able to observe very weak hyperfine satellite lines in the 18-16 vibration-rotation transitions. Examples of the weak transitions, which correspond to $\Delta G_2 = \pm 1, \pm 2$, are shown in figure 10, together with the corresponding experimental spectrum. Analysis provides values of the deuteron Fermi contact constant for both vibrational levels, which are listed in table 3. As anticipated, they are very close to one half of the free-atom value (109 MHz), confirming that for $v = 16$ and 18 the electron density distribution is essentially symmetrical.

An even more interesting situation arises for transitions which involve vibrational levels very close to the dissociation limit, particularly $v = 21$ and 22. We have already noted (figure 8) that rotational components of the 21-17 (Carrington *et al* 1988b) and

**Table 3.** Comparison of experimental and theoretical proton and deuteron Fermi contact hyperfine constants in vibration-rotation levels of $HD^+$. The dissociation energies are those calculated by Wolniewicz and Poll (1986), except for $v = 22$ which are from Carrington *et al* (1988f). Theoretical hyperfine constants are from Carrington and Kennedy (1985) and Kennedy *et al* (1988). Electron densities are obtained by dividing the experimental Fermi contact hyperfine constants by the free atom values. For $v = 16$ and 18 the experimental data were analysed by neglecting the rotational dependence of the hyperfine constants; the dissociation energies listed are for the $N = 0$ levels.

| | | | Experiment | | | | Theory | | Density | |
|---|---|---|---|---|---|---|---|---|---|---|
| | | | $b_{1F}$ (MHz) | | $b_{2F}$ (MHz) | | | | | |
| $v$ | $N$ | $E$(diss) ($cm^{-1}$) | IR | RF | IR | RF | $b_{1F}$ (MHz) | $b_{2F}$ (MHz) | $\rho_1$ | $\rho_2$ |
| 16 | | (1514.327) | — | — | 110.7 | — | 719.7 | 111.7 | — | 0.508 |
| 18 | | (598.115) | — | — | 109.8 | — | 704.8 | 111.6 | — | 0.504 |
| 17 | 0 | 1007.089 | 719.5 | — | 112.4 | — | 713.3 | 111.4 | 0.507 | 0.515 |
| | 1 | 994.551 | 718.3 | 711.90 | 112.9 | 111.14 | 713.1 | 111.4 | 0.506 | 0.518 |
| | 2 | 969.653 | 718.6 | 711.6 | 112.1 | 111.6 | 712.6 | 111.3 | 0.506 | 0.514 |
| | 3 | 932.750 | 717.2 | — | 113.0 | — | 711.8 | 111.3 | 0.505 | 0.518 |
| | 4 | 884.367 | 716.7 | — | 112.7 | — | 710.8 | 111.2 | 0.505 | 0.517 |
| 21 | 0 | 10.210 | 137.0 | — | 198.0 | — | 145.6 | 196.0 | 0.096 | 0.899 |
| | 1 | 8.553 | 123.0 | — | 202.6 | — | 126.4 | 199.0 | 0.087 | 0.913 |
| | 2 | 5.560 | 85.6 | — | 206.4 | — | 91.3 | 204.3 | 0.060 | 0.937 |
| | 3 | 1.820 | 46.7 | 47.59 | 212.4 | 211.38 | 48.2 | 211.0 | 0.033 | 0.968 |
| 22 | 0 | 0.438 | 16.4 | — | 217.6 | — | 11.1 | 216.7 | 0.012 | 0.994 |
| | 1 | 0.123 | 7.4 | — | 218.3 | — | 5.5 | 217.6 | 0.005 | 0.998 |

**Table 4.** Experimental and theoretical hyperfine constants for $H_2^+$ (MHz). Experimental values are taken from Jefferts (1969). Theoretical values are from McEachran *et al* (1978).

| | $N = 1$ | | | | | | $N = 2$ | |
|---|---|---|---|---|---|---|---|---|
| | $b_F$ | | $t$ | | $\gamma$ | | $\gamma$ | |
| $v$ | Expt | Theory | Expt | Theory | Exp | Theory | Expt | Theory |
| 4 | 836.743 | 838.036 | 32.678 | 32.751 | 32.636 | 32.640 | 32.448 | 32.434 |
| 5 | 819.239 | 820.488 | 30.393 | 30.463 | 30.421 | 30.423 | 30.240 | 30.226 |
| 6 | 803.186 | 804.392 | 28.180 | 28.246 | 28.266 | 28.267 | 28.092 | 28.079 |
| 7 | 788.519 | 789.684 | 26.025 | 26.087 | 26.156 | 26.158 | 25.991 | 25.942 |
| 8 | 775.182 | 776.310 | 23.911 | 23.971 | 24.080 | 24.082 | 23.922 | 23.910 |

22-17 (Carrington *et al* 1988f) bands exhibit well resolved hyperfine patterns, and this is because the hyperfine splittings in the lower and upper states are very different. Vibration-rotation levels which lie close in energy to the lower dissociation limit, $H^+ + D$, possess an electron distribution which becomes increasingly asymmetric as dissociation is approached, with the result that the proton Fermi contact constant decreases, and the deuteron constant increases. For such levels the $G_1$, $G_2$ coupling scheme described earlier becomes inappropriate, and hyperfine components of the vibration-rotation transitions which involve $\Delta G_1 = \pm 1$ become intense. In addition

the diagonal $\Delta G_1 = 0$ transitions are well separated because of the different hyperfine splittings in the lower and upper states. The result is that the 21–17 and 22–17 vibration–rotation transitions all show a similar six-line structure, with further subsidiary splittings and weak lines. These can be analysed fairly completely, to yield the Fermi contact hyperfine constants given in table 3. The highest bound vibration–rotation level (22, 1) has a dissociation energy of only $0.123\ \mathrm{cm}^{-1}$ and an average internuclear distance of almost 22 Å. In this level the $HD^+$ molecule is best described as a deuterium atom interacting very weakly with a long-range proton: the electron is almost wholly associated with the deuterium nucleus.

### *4.4. Radiofrequency and microwave spectra of $HD^+$ and $H_2^+$*

The best method of determining the nuclear hyperfine constants in $HD^+$ would be to observe directly the transitions between hyperfine levels in particular vibration–rotation levels, and Carrington *et al* (1989a) have recently succeeded in such experiments using a radiofrequency/infrared double resonance method. The necessary modifications to the ion beam apparatus are shown in figure 11; the drift tube for Doppler tuning of the infrared transition is replaced by a radiofrequency cell consisting of a central copper rod placed inside a copper cylinder. The cell is designed to have an impedance of 50 Ω, to operate up to a frequency of 1000 MHz, and to transmit at least 10 W of radiofrequency power over this range. The ion and laser beams pass between the centre and outer conductors of the radiofrequency cell. The ion source potential is adjusted to the value necessary for a particular hyperfine component of a vibration–rotation transition to be driven by the infrared laser, and the proton fragments produced by electric field dissociation of the upper state are monitored as before. Hyperfine transitions involving the pumped level are now simultaneously driven by the radiofrequency magnetic field, and they result in an increased proton fragment ion yield. We are able to observe both lower and upper state double resonance transitions, and therefore to determine accurate values (table 3) of the nuclear hyperfine constants for the vibration–rotation levels approaching the $HD^+$ dissociation limit.

The radiofrequency spectra we have observed for $HD^+$ by the double resonance method are similar in type to those observed by Jefferts (1969) for $H_2^+$, which involved the vibrational levels $v = 4$ to 8. Figure 4 shows the fine and hyperfine splitting of the $N = 1$ and 2 levels of $H_2^+$, and the radiofrequency transitions observed by Jefferts. The hyperfine constants determined by him are listed in table 4, and are compared with theoretical predictions.

Similar double resonance experiments using microwave radiation have been described by Carrington *et al* (1989c). The rotational transition, 22,1–22,0, involving the last two bound levels of $HD^+$, is predicted to occur at a frequency close to 9.5 GHz. The apparatus shown in figure 11 was modified by including a short drift tube after lens 1 and replacing the radiofrequency cell by a microwave cell. Each nuclear hyperfine level in the $v = 22$, $N = 1$ level is populated in turn by infrared excitation from 17,2, and in each case the corresponding hyperfine component of the rotational transition to 22,0 is driven by the microwave electric field. The transitions involved and spectra are shown in figure 12. The electric field dissociation lens and following magnetic analyser can be set to collect protons formed by the field dissociation of 22,1, in which case the observed microwave lines correspond to a decrease in the proton current. Alternatively, the lens and magnetic analyser can be adjusted to collect protons from the fragmentation of 22,0, and in this case the microwave signals are observed as an

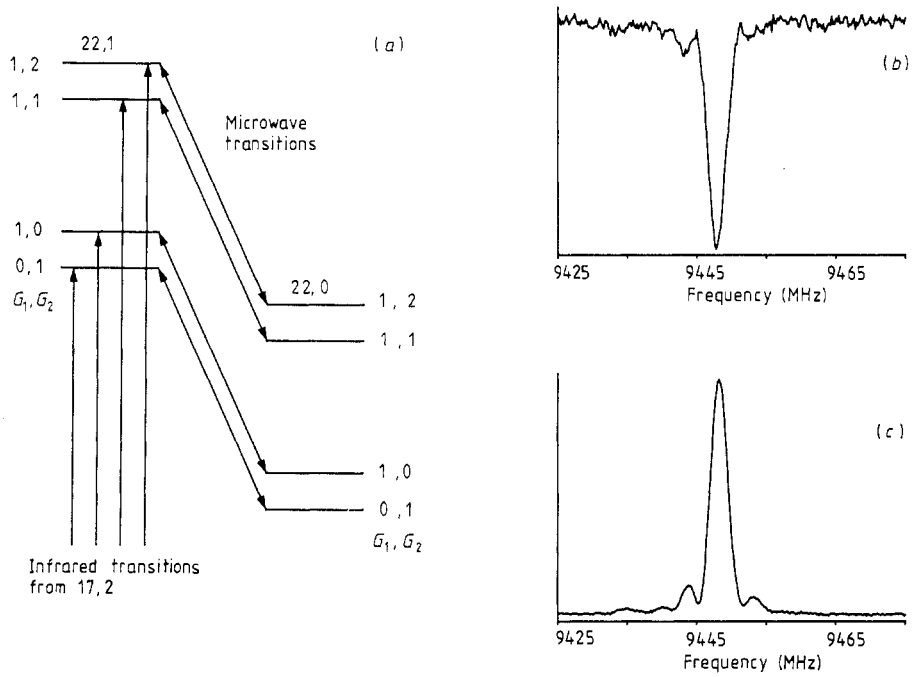


**Figure 12.** (*a*) Nuclear hyperfine splitting of the 22,1 and 22,0 vibration-rotation levels of $HD^+$, showing the observed microwave transitions. (*b*) Microwave/infrared double resonance line (22,1-22,0) obtained by measuring a resonant decrease in the number of fragment $H^+$ ions produced by electric field dissociation of 22,1. (*c*) The same double resonance line as shown in (*b*), but recorded by measuring a resonant increase in the number of fragment $H^+$ ions produced by electric field dissociation of 22,0.

increased proton fragment current. The electric field dissociation method is therefore shown to be capable of discriminating between two levels which are separated by only 0.3 $cm^{-1}$.

## 5. Electronic spectra of the $D_2^+$ and $H_2^+$ ions

We have not so far discussed the first excited electronic state ($2p\sigma_u$) of $H_2^+$ in detail, except to comment that it is essentially repulsive. The consequent photodissociation has been seen to be crucial in the radiofrequency studies of $H_2^+$ and in the infrared studies of $HD^+$. However, it is important to realise that the $2p\sigma_u$ state is not repulsive for all values of the internuclear distance. It has been appreciated for many years that when a proton approaches a hydrogen atom, the charge distribution of the atom is polarised, resulting in an electrostatic interaction with the proton. This interaction was first examined theoretically by Coulson (1941), who determined the coefficients of the electrostatic multipole expansion and showed that the leading term has the form $-\alpha/8\pi\varepsilon_0 R^4$, where $\alpha$ is the polarisability of the hydrogen atom. This term represents the charge/induced-dipole interaction, and its effect is to lower the potential energy of the $H+H^+$ system as $R$ decreases, until the valence or exchange forces become dominant. The result is that in $H_2^+$, $D_2^+$ and $HD^+$ the $2p\sigma_u$ state is predicted to have a shallow potential minimum at $R = 6.6$ Å with a Born-Oppenheimer well depth of

13.34 $cm^{-1}$. In all three ions this potential well is expected to support a small number of vibration-rotation levels, so that a discrete electronic spectrum arising through transitions from the $1s\sigma_g$ ground state is possible. We have recently observed such a spectrum for the $D_2^+$ ion. It should be stressed that the long-range minimum (described as a van der Waals complex by Coulson) also arises naturally from the solution of the electronic Schrödinger equation to give the Born-Oppenheimer potential.

The only previously published theoretical values of the van der Waals vibration-rotation levels for $H_2^+$ were those of Peek (1969), using the Born-Oppenheimer potential. Although Peek commented on the existence of the corresponding levels for $D_2^+$, with the prediction that $v = 0$, $N = 0$ to 4 and $v = 1$, $N = 0$ and 1 would be bound, he did not calculate the vibration-rotation energies. The calculations of Carrington *et al* (1989d) using the standard adiabatic potential confirmed the prediction of seven bound levels for $D_2^+$, the lowest level ($v = 0$, $N = 0$) having a calculated binding energy of 5.513 $cm^{-1}$, and the highest ($v = 1$, $N = 1$) having a binding energy of 0.147 $cm^{-1}$. It was apparent to us that the 0-21 and 1-21 bands of the $D_2^+$ $2p\sigma_u$-$1s\sigma_g$ electronic spectrum should lie in the infrared region spanned by the $CO_2$ laser. The potential curves and relevant vibration-rotation levels for both states are shown in figure 13. Of the nine predicted rotational components of the 0-21 band we have observed seven, and we have also observed all three predicted components of the 1-21 band (Carrington *et al* 1988g, 1989d). The potential curves shown in figure 13 suggest that the Franck-Condon factors for the infrared transitions are likely to be very small, and these expectations are confirmed by calculations of the vibrational wavefunctions using the standard adiabatic potential. The experiments succeed because of the use of a focused cw laser beam, combined with the electric field dissociation of the $2p\sigma_u$ levels, which provides an extremely sensitive method of detection.

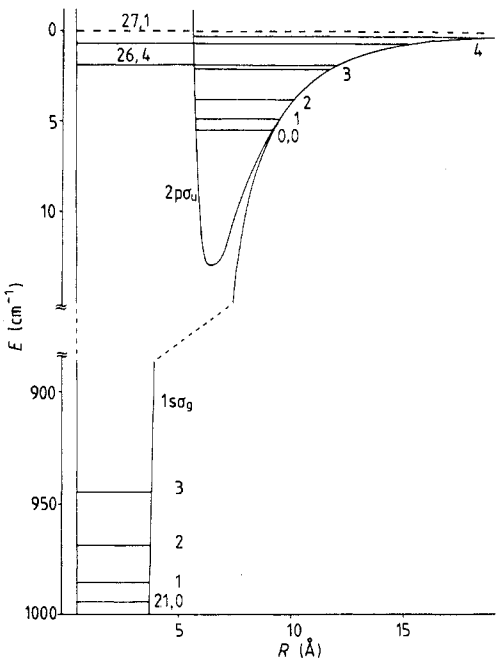


**Figure 13.** Adiabatic potential energy curves, and relevant vibration-rotation levels, for the ground and first excited electronic states of $D_2^+$ in the region of the dissociation limit.

As the potential energy curves given in figure 13 indicate, the highest energy vibration-rotation levels of the ground state should lie very close in energy to the van der Waals levels, so that some transitions between the levels of the two electronic states can be expected to occur at rather low frequencies. We have observed two such transitions for $D_2^+$ which occur in the microwave region of the spectrum (Carrington *et al* 1989c). Figure 14 shows examples of infrared and microwave absorption lines, detected by electric field dissociation. We detected the first microwave lines by infrared/microwave double resonance studies, but were subsequently able to detect one of the microwave transitions (0,3-26,4) without the population enhancement provided by simultaneous infrared excitation. The results showed, very surprisingly, that for the levels studied in our experiments, the population in the ion beam of the van der Waals level 0,3 is higher than that of the high-lying ground-state level 26,4. Analysis of the infrared and microwave spectra confirmed the main predictions of the adiabatic calculations; table 5 summarises our knowledge of the energy levels, molecular constants and bond lengths for the $D_2^+ 2p\sigma_u$ van der Waals state. An important conclusion arising from our studies of the $D_2^+$ ion, particularly from the absence of resolved nuclear hyperfine splitting, is that the inversion symmetry is preserved, even

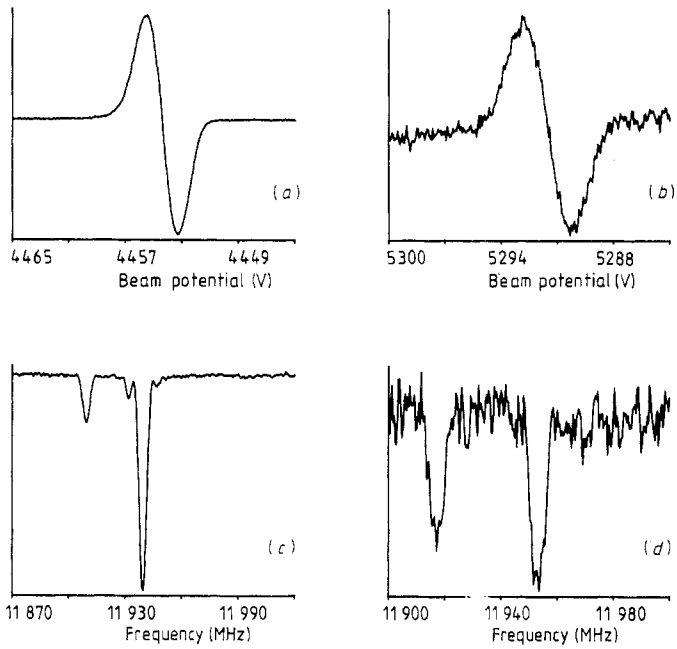


**Figure 14.** (*a*) $D_2^+ 2p\sigma_u$ 0,2-$1s\sigma_g$ 21,1 infrared transition obtained by Doppler modulation and tuning of the ion beam, combined with electric field dissociation of the 0,2 level and detection of the resulting $D^+$ fragments. (*b*) $D_2^+ 2p\sigma_u$ 1,0-$1s\sigma_g$ 21,1 infrared transition obtained by Doppler modulation and tuning of the ion beam, combined with electric field dissociation of the 1,0 level. (*c*) $D_2^+ 2p\sigma_u$ 0,3-$1s\sigma_g$ 26,4 microwave/infrared double resonance line obtained by monitoring $D^+$ fragments from the electric field dissociation of the 0,3 level. Amplitude modulation of the microwave power is used with phase-sensitive detection. (*d*) $D_2^+$ 0,3-26,4 transition obtained by pure microwave spectroscopy, monitoring the electric field dissociation of 0,3. Note the inverted phase of the line, showing that microwave excitation results in a decrease in the 0,3 population. The doubling of the lines shown in (*c*) and (*d*) is due to back-reflected microwave power.

**Table 5.** Vibration-rotation levels and molecular constants for the $D_2^+$ $2p\sigma_u$ long-range van der Waals state.

| Dissociation energies ($cm^{-1}$) | | | | | |
|---|---|---|---|---|---|
| | $N=0$ | 1 | 2 | 3 | 4 |
| $v=0$ | −5.513 | −4.952 | −3.853 | −2.280 | −0.356 |
| $v=1$ | −0.308 | −0.147 | | | |
| **Rotational constants and bond lengths** | | | | | |
| $v=0$ | $B_0=0.282\,49\ cm^{-1}$ | | $R_0=7.7$ Å | | |
| $v=1$ | $B_1=0.086\,54\ cm^{-1}$ | | $R_1=13.9$ Å | | |
| **Vibrational and equilibrium constants** | | | | | |
| $\Delta G_{1/2}=5.205\ cm^{-1}$ | | $\omega_e=20.09\ cm^{-1}$ | $D_e=13.346\ cm^{-1}$ | | $R_e=6.64$ Å |

in the highest vibration-rotation levels, of both the ground and first excited electronic states.

Peek (1969) has predicted that $H_2^+$ in its long-range $2p\sigma_u$ state possesses four bound vibration-rotation levels. An electronic spectrum of $H_2^+$ similar to that described above for $D_2^+$ must, in principle, be observable, but unfortunately it is not predicted to have vibrational bands in the carbon dioxide infrared laser region. Pure microwave transitions similar to those in $D_2^+$ are accessible, however, and Carrington *et al* (1989b) have recently detected a transition in $H_2^+$ at 17 607 MHz. This spectroscopic line arises from the 0,2-19,1 vibration-rotation component of the $2p\sigma_u$-$1s\sigma_g$ electronic transition; it is detected by electric field dissociation of the $2p\sigma_u$ 0,2 state, which has a dissociation energy of 0.807 $cm^{-1}$. The $1s\sigma_g$ 19,1 level is the highest bound ground-state level of $H_2^+$, with a dissociation energy of 0.215 $cm^{-1}$. As in the case of $D_2^+$, the van der Waals level (0,2) is found to have the higher population in the ion beam. This microwave transition is the only one accessible with the microwave sources available to us at present, but other components of the $2p\sigma_u$-$1s\sigma_g$ electronic transition are predicted to occur at much higher frequencies in the microwave and far-infrared regions. A number of theoretical transition frequencies are listed by Carrington *et al* (1989b), and these, together with the laboratory frequency listed above, may be of value in searches for extraterrestrial $H_2^+$. Ionisation of $H_2$ by ultraviolet radiation or cosmic-ray particles is thought to be of primary importance in the initiation of interstellar chemistry, but extraterrestrial $H_2^+$ has not yet been discovered, despite a number of searches for its radiofrequency magnetic-dipole transitions.

The experimental problems which arise in attempts to study the corresponding electronic spectrum of $HD^+$ are discussed in the final section.

## 6. Conclusions

This review has been concerned with studies of the spectra of the three isotopic relations $H_2^+$, $D_2^+$ and $HD^+$. It would be possible to carry out similar investigations of the molecular ions containing tritium, but it is not clear that important new information

would be obtained. The vibration-rotation levels of the ground electronic state of $HD^+$ have now been studied very thoroughly by both experiment and theory. The increasing asymmetry of the molecular wavefunction as we approach the lowest dissociation limit is now well understood, particularly as a result of the study of nuclear hyperfine interactions. The long-range $2p\sigma_u$ state of $D_2^+$ has been studied in considerable detail, through electronic excitations from high vibrational levels of the ground state, and information about the molecular constants in this unusual state obtained. The long-range $2p\sigma_u$ state of $H_2^+$ has also been identified, through the observation of an electronic transition occurring in the microwave region. Finally the proton hyperfine interactions in a number of different vibrational levels of $H_2^+$ have been measured by radiofrequency experiments combined with quadrupole trapping.

A number of possible spectroscopic investigations remain to be attempted. The heteronuclear species $HD^+$ is also predicted to exhibit a long-range $2p\sigma$ minimum, supporting several vibration-rotation levels. However, the $2p\sigma$ state correlates with the $H+D^+$ upper dissociation limit, and the van der Waals levels lie above the lower $H^+ + D$ dissociation limit. They are therefore able to predissociate, and calculations of their lifetimes by Davis and Thorson (1978) lead to predicted spectroscopic linewidths of several wavenumbers. If these predictions are correct, the $2p\sigma$–$1s\sigma$ spectrum of $HD^+$ is almost certainly unobservable by our methods.

The only reported spectroscopic investigations of $H_2^+$ itself are the radiofrequency and microwave studies described in this review; none of its vibration-rotation frequencies have yet been determined experimentally. The same is true of the $D_2^+$ molecule, except that some information about the rotational spacings in $v = 21$ is obtained from the electronic spectrum described earlier. We have investigated theoretically the possibility of observing electric quadrupole vibration-rotation spectra of $H_2^+$ and $D_2^+$, and although these transitions are predicted to be some nine orders of magnitude weaker than the electric dipole transitions in $HD^+$, we believe we are close to achieving the sensitivity necessary for their detection. Two other experiments involving $H_2^+$ or $D_2^+$ are under consideration at present. An electric field will mix the $1s\sigma_g$ and $2p\sigma_u$ states, so that vibration-rotation transitions involving levels close to the dissociation limit should acquire electric dipole intensity, whilst still satisfying quadrupole selection rules. An applied electric field effectively removes the centre of inversion, and an asymmetric electron distribution, even in $H_2^+$, might be observable. A second possible route to the study of the homonuclear molecules has been suggested to us by Kennedy (1988); it might be possible to use two infrared lasers, at different frequencies and aligned parallel and antiparallel to the ion beam, to induce two-photon transitions which involve the repulsive $2p\sigma_u$ electronic state as an intermediate.

Madsen and Peek (1971) have carried out extensive Born-Oppenheimer calculations of many of the excited electronic states of the hydrogen molecular ion. Apart from the ground electronic state, theory predicts two other electronic states which are bound, the $3d\sigma_g$ and $2p\pi_u$ states, lying approximately 11 eV above the ground state. Although all of the other excited electronic states are essentially repulsive, many of them are predicted to exhibit long-range minima similar in origin to that discussed here for the $2p\sigma_u$ state. Since the polarisability of the hydrogen atom increases with electronic excitation, these potential minima are much deeper and occur at even larger internuclear distances than for the $2p\sigma_u$ state (Coulson and Gillam 1948). No direct experimental spectroscopic studies have been described for any of these excited states, in any of the possible isotopic species, but recent translational energy-loss studies of $H_2^+$ have provided experimental confirmation of the $2p\pi_u$ state (Kirchner *et al* 1984).

Our experimental studies of $HD^+$, $D_2^+$ and $H_2^+$ have led to successive refinements of the theory, and we now believe that for the ground state of $HD^+$ the non-adiabatic, relativistic and radiative contributions are well understood. We hope to be able to report further experimental studies, particularly of the homonuclear molecules. We also believe that the experimental techniques developed in our efforts to obtain spectra of the hydrogen molecular ion can be extended to other molecular ions.

## Acknowledgments

The theoretical work of Dr R A Kennedy has been crucial to the success of many of our experiments, and we are grateful to him for supplying results prior to their publication. AC thanks the Royal Society for a Research Professorship, IRM thanks the University of Southampton for a Research Fellowship, and CAM thanks the British Petroleum Company plc for a research studentship. We are also indebted to the SERC who have supported our experimental work.

## References

Bishop D M 1974 *Mol. Phys.* **28** 1397
Bishop D M and Cheung L M 1977 *Phys. Rev.* A **16** 640
Bjerre N and Keiding S R 1986 *Phys. Rev. Lett.* **56** 1459
Born M and Huang K 1954 *Dynamical Theory of Crystal Lattices* (London: Oxford University Press) Appendix VIII
Carrington A and Buttenshaw J 1981 *Mol. Phys.* **44** 267
Carrington A, Buttenshaw J and Kennedy R A 1983 *Mol. Phys.* **48** 775
Carrington A, Buttenshaw J and Roberts P G 1979 *Mol. Phys.* **38** 1711
Carrington A and Kennedy R A 1984 *Gas Phase Ion Chemistry* vol 3 *Ions and Light* ed M T Bowers (London: Academic) pp 393-442
—— 1985 *Mol. Phys.* **56** 935
Carrington A, McNab I R and Montgomerie C A 1987 *J. Chem. Phys.* **87** 3246
—— 1988a *Phil. Trans. R. Soc.* A **324** 275
—— 1988b *Mol. Phys.* **64** 983
—— 1988c *Chem. Phys. Lett.* **149** 326
—— 1988d *Chem. Phys. Lett.* **151** 258
—— 1988e *Mol. Phys.* **64** 679
—— 1988f *Mol. Phys.* **65** 751
—— 1988g *Phys. Rev. Lett.* **61** 1573
—— 1989a *Mol. Phys.* **66** 519
—— 1989b *Chem. Phys. Lett.*, **160** 237
Carrington A, McNab I R, Montgomerie C A and Brown J M 1989c *Mol. Phys.* **66** 1279
Carrington A, McNab I R, Montgomerie C A and Kennedy R A 1989d *Mol. Phys.* **67** 711
Cooley J W 1961 *Math. Comput.* **15** 363
Coulson C A 1941 *Proc. R. Soc. Edinburgh* A **61** 20
Coulson C A and Gillam C M 1948 *Proc. R. Soc. Edinburgh* A **62** 360
Dalgarno A, Patterson T N L and Somerville W B 1960 *Proc. R. Soc.* A **259** 100
Davis J P and Thorson W R 1978 *Can. J. Phys.* **56** 996
Dehmelt H G and Jefferts K B 1962 *Phys. Rev.* **125** 1318
Dunn G H 1966 *J. Chem. Phys.* **44** 2592
Frosch R A and Foley H M 1952 *Phys. Rev.* **88** 1337
Hiskes J R 1961 *Phys. Rev.* **122** 1207
Hunter G and Pritchard H O 1967 *J. Chem. Phys.* **46** 2146, 2153
Hunter G, Yau A W and Pritchard H O 1974 *At. Data Nucl. Data Tables* **14** 11
Hylleraas E A 1931 *Z. Phys.* **71** 739

Jaffé G 1934 *Z. Phys.* **87** 535
Jefferts K B 1968 *Phys. Rev. Lett.* **20** 39
—— 1969 *Phys. Rev. Lett.* **23** 1476
Kaufman S L 1976 *Opt. Commun.* **17** 309
Kennedy R A 1988 private communication
Kennedy R A, Moss R E and Sadler I A 1988 *Mol. Phys.* **64** 177
Kirchner N J, O'Keefe A, Gilbert J R and Bowers M T 1984 *Phys. Rev. Lett.* **52** 26
Kohl D A and Shipsey E J 1986 *J. Chem. Phys.* **84** 2707
McEachran R P, Veenstra C J and Cohen M 1978 *Chem. Phys. Lett.* **59** 275
Madsen M M and Peek J M 1971 *At. Data* **2** 171
Moss R E 1973 *Advanced Molecular Quantum Mechanics* (London: Chapman and Hall) pp 137-143
Moss R E and Sadler I A 1987 *Mol. Phys.* **61** 905
—— 1988 *Mol. Phys.* **64** 165
—— 1989 *Mol. Phys.* **66** 591
Pack R T 1985 *Phys. Rev.* A **32** 2022
Peek J M 1969 *J. Chem. Phys.* **50** 4595
Richardson C B, Jefferts K B and Dehmelt H G 1968 *Phys. Rev.* **165** 80
Riviere A C and Sweetman D R 1960 *Phys. Rev. Lett.* **5** 560
Struensee M C, Cohen J S and Pack R T 1986 *Phys. Rev. A* **34** 3605
Tadjeddine M and Parlant G 1977 *Mol. Phys.* **33** 1797
Teller E and Sahlin H L 1970 *Physical Chemistry: An Advanced Treatise* vol V (New York: Academic) pp 35-124
Wind H 1964 *Proc. Phys. Soc.* **84** 617
—— 1966 *Nucl. Fusion* **6** 67
Wing W H, Ruff G A, Lamb W E and Spezeski J J 1976 *Phys. Rev. Lett.* **36** 1488
Wolniewicz L and Poll J D 1978 *J. Mol. Spectrosc.* **72** 264
—— 1980 *J. Chem. Phys.* **73** 6225
—— 1985 *Can. J. Phys.* **63** 1201
—— 1986 *Mol. Phys.* **59** 953
—— 1989 *Mol. Phys.* **66** 701